MATHEMATISCHES FORSCHUNGSINSTITUT OBERWOLFACH

Report No. 24/2006

Mathematical Biology

Organised by
Emmanuele DiBenedetto (Vanderbilt University, Nashville)
Benoît Perthame (École Normale Supérieure, Paris)
Angela Stevens (Max-Planck-Institute for Mathematics in the Sciences, Leipzig)

May 14th – May 20th, 2006

ABSTRACT. This years meeting on Mathematical Biology focussed on the mathematical modeling and analysis of some specific bio-medical questions, where quite detailed experimental findings are available. A main aim for this decision was to further deepen the exchange between the fields, on the long run in a similar manner as known e.g. from mathematics and physics. Talks by mathematicians and talks by experimentalists on related scientific questions were put back to back, wherever possible.

Introduction by the Organisers

This meeting on Mathematical Biology tied in with the long tradition of these workshops in Oberwolfach and at the same time aimed to account for the fast growing synergy between biology and mathematics of the recent years. The use of new instrumentation and visualization methods at the molecular scale in biological and medical experiments allows for measurements which have not been possible a few years ago. Major questions for theoreticians and experimentalists are how to tackle this vast complexity of biological information and data, and, more important, if underlying principles can be found. Finding these would enable the field to become more predictive. Here is exactly where mathematical modeling, analysis, and simulation can contribute. On the other hand, mathematical biologists and mathematicians are now providing first new models to explain the measurements, and these models are ready for mathematical analysis.

The synergy between mathematics and physics, chemistry, engineering, and material sciences, has already proven to greatly advance the respective sciences and mathematics itself. To further deepen the connections between mathematics and

biology, a group of experimental biologists, mathematical biologists, and mathematicians - especially many young scientists - met, joining the lively talks and discussions in this workshop.

The meeting intentionally focussed on some specific biological topics this time. Among those were cell movement, where results on the dynamics of the cellular cytoskeleton were presented, as well as on chemotaxis and cell adhesion. Questions of pattern and structure formation in cell systems were discussed for self-organizing microorganisms and cancer invasion. The analysis of structured population models in this context is new, but has a long tradition in ecology and epidemiology. Further topics of interest with clear mathematical challenges were transport and molecular motors, the organization of cell membranes, and the process of phototransduction

Wherever possible, the experimentalists talks were placed in tandem with related presentations on mathematical modeling.

Mathematical topics were: reaction-diffusion equations, parabolic and hyperbolic chemotaxis equations, fluid dynamics, variational principles and methods based on the Wasserstein distance, homogenization, singular perturbations, bifurcation analysis, and numerical simulations.

Besides the lectures, two discussion groups were organized, one on mathematical results for chemotaxis equations and one on cell motility. A round table discussion on 'mathematical modeling in biology, aims and scopes' rounded off the meeting, not to forget the nice concert, organized by some of the participants.

We would like to express our sincere thanks to the very dynamic and kind support of the Oberwolfach team before and during the workshop.

Workshop: Mathematical Biology

Table of Contents

Abstracts

Control of actin assembly in cell motility
Marie-France Carlier

Living cells change shape and move in response to environmental signals. Motile processes play a pivotal role in morphogenesis, migration of embryonic and metastasis cells, angiogenesis, synaptic plasticity, immune response and interaction of the host cells with pathogens. They are generated by polarized, spatially directed actin assembly in filaments organized in specific structures. Protrusive force at the leading edge as well as tensile forces at focal contacts are produced by barbed end growth of actin filaments, locally stimulated at the membrane and globally inhibited in solution. The number of filaments and the rate of barbed end growth, fed by the treadmilling of actin filaments, determines the force. These parameters are controlled by protein machineries that initiate filaments in a spatially restricted fashion either by nucleation or by end branching, and by proteins that bind monomeric actin in a complex that has specific assembly rate parameters.

Two protein machineries are responsible for spatially directed initiation of actin filaments. They operate with different mechanisms and in distinct processes, 1) the WASP-Arp2/3 system is at the origin of the formation of a branched filament array responsible for protrusion of lamellipodium; 2) formins, in association with profilin, catalyze the rapid processive assembly of non-branched actin filaments arranged in parallel bundles, in the cytokinetic ring and in adhesive structures. We have combined a biochemical and a biomimetic approach to understand the molecular mechanisms of these auto-organized processes. We have reconstituted the sustained actin-based movement of a N-WASP- or formin-functionalized solid particle or giant liposome in a biochemically controlled medium, which enables measurements of force production in correlation with structure and motility, and we can derive informations on the molecular mechanism of movement by single molecule measurements. The dependence of continuous or saltatory (periodic) movement on the solution components has been analyzed for solid particles and liposomes.

References

[1] T. Loisel, R. Boujemaa, D. Pantaloni and M.F. Carlier, *Reconstitution of actin-based movement using pure proteins*, Nature **401** (1999), 613–616.

[2] D. Pantaloni, R. Boujemaa, D. Didry, P. Gounon and M.F. Carlier, *Arp2/3 complex branches filament barbed ends: Functional antagonism with capping proteins*, Nature Cell Biology **2** (2000), 385–391.

[3] D. Pantaloni, C. Le Clainche and M.F. Carlier, *Mechanism of actin-based motility*, Symposium "Novel Perspectives in Cell Motility", Science **292** (2001), 1502–1506.

[4] S. Wiesner, E. Helfer, D. Didry, G. Ducouret, F. Lafuma, M.F. Carlier, D. Pantaloni, *A biomimetic motility assay provides insight into the mechanism of actin-based motility*, J. Cell. Biol. **160** (2003), 387–98.

[5] S. Romero, C. Le Clainche, D. Didry, C. Egile, D. Pantaloni and M.F. Carlier, *Formin is a processive motor that requires profilin to accelerate actin polymerization and ATP hydrolysis*, Cell **119** (2004), 419–429.

Models for Hard and Soft Particle Propulsion by Actin-Based Motility

RICHARD B. DICKINSON

(joint work with Daniel L. Purich)

Invasive pathogens (such as Listeria monocytogenes) and vesicles can be propelled intracellularly by actin polymerization in a mechanism that remains controversial and poorly understood. Several recent studies have examined the propulsion of particles such as polystyrene microspheres, oil droplets, and vesicles, under relatively well-defined conditions in vitro. Propulsion requires particles to be coated with filament-nucleation protein factors such as Listeria ActA, N-WASP (neural Wiskott-Aldrich Syndrome Protein), or the N-WASP VCA domain, which polymerize actin filaments from the particles surface to generate a dense F-actin "rocket tail", similar to that formed by invasive intracellular microorganisms like Listeria. There is increasing evidence that these surface-bound factors also play a role in facilitating (+)-end assembly following filament nucleation [1, 2, 3, 4] (ActA by its interaction with Vasodilator-Stimulated Phosphoprotein or VASP).

Based on thermodynamic, mechanical, and kinetic arguments and supporting mathematical models, we have previously proposed that the dominate mechanism of polymerization actin-based motility is by filament end-tracking motors, which are particle surface-bound proteins that tether the elongating filament end and facilitate monomer addition in a force-insensitive manner [1, 5]. In this view, the propelled particle is in a quasi-static equilibrium between the forces caused compressed versus tense filaments, and other forces on the propelled particle (e.g. hydrodynamic drag forces) are comparatively negligible. Filaments in the different compressed or tense states can arise simply from stochastically variable elongation rates, or, for larger particles, from the monomer concentration gradients that are created by local consumption of monomers at the surface. Our proposed filament end-tracking motor mechanism is fundamentally different from the conventional view the filaments push by a free-filament thermal ratchet mechanism [6, 7], in which working filaments must be free to add subunits and the resistance to propulsion and attachment to the generated actin network are caused by other mechanism(s).

Under the key assumption of force-insensitive elongation of (+)-end-tethered actin filaments, our filament-scale and continuum modeling of the actin network and reaction-diffusion models for monomer consumption by end-tracking motors is sufficient to fully recapitulate the key experimental observations of particle propulsion by actin based motility: (1) stepwise motion, small fluctuations, rotation and helical paths of Listeria trajectories; (2) the dependence of particle velocity on particle radius; (3) the critical radius for saltatory motion of biomimetic hard particles; and (4) evolution of biomimetic soft particles (vesicles and oil drops) into

teardrop shapes as well as the observed periodic distension and round of these shapes.

REFERENCES

[1] R.B. Dickinson, and D.L. Purich, *Clamped-filament elongation model for actin-based motors*, Biophys J. **82** (2002), 605–17.

[2] D. Chereau, F. Kerff, P. Graceffa, Z. Grabarek, K. Langsetmo and R. Dominguez, *Actin-bound structures of Wiskott-Aldrich syndrome protein (WASP)-homology domain 2 and the implications for filament assembly*, Proc Natl Acad Sci USA **102** (2005), 16644–9.

[3] J.E. Bear, T.M. Svitkina, M. Krause, D.A. Schafer, J.J. Loureiro, G.A. Strasser, I.V. Maly, O.Y. Chaga, J.A. Cooper, G.G. Borisy and F.B. Gertler, *Antagonism between Ena/VASP proteins and actin filament capping regulates fibroblast motility*, Cell **109** (2002), 509–21.

[4] M. Barzik, T.I. Kotova, H.N. Higgs, L. Hazelwood, D. Hanein, F.B. Gertler and D.A. Schafer, *Ena/VASP proteins enhance actin polymerization in the presence of barbed end capping proteins*, J Biol Chem **280** (2005), 28653–62.

[5] R.B. Dickinson, L. Caro and D.L. Purich, *Force generation by cytoskeletal filament end-tracking proteins*, Biophys J **87** (2004), 2838–54.

[6] A. Mogilner and G. Oster, *Cell motility driven by actin polymerization*, Biophys J **71** (1996), 3030–45.

[7] A. Mogilner and G. Oster, *Force Generation by Actin Polymerization II: The Elastic Ratchet and Tethered Filaments*, Biophys J. **84** (2003), 1591–605.

Control of integrin clustering by nanopatterned interfaces and micromechanical devices

ACHIM BESSER

(joint work with Patrick Heil, Ada Cavalcanti-Adam, Marco Arnold, Joachim P. Spatz)

Focal adhesions are micrometer-sized protein aggregates that connect the actin cytoskeleton to the extracellular matrix (ECM). The essential link through the plasma membrane is provided by the transmembrane protein integrin. Integrin is on the one hand connected via an elaborated architecture of plaque proteins [1] to actin filaments and on the other hand binds to extracellular proteins offering the RGD-sequence. It is known that the integrin protein exists in a variety of active and inactive conformations [2] and that it has to be activated to promote focal adhesion formation.

To investigate molecular details of integrin clusters one has to provide an experimental method to control the interface between a cell and the ECM on a nanometer length scale. Our approach is to use nanostructured, biofunctionalized surfaces that mimic the ECM. However, in order to get significant statistics in a biological assay one has to observe at least 100 cells under the same experimental conditions which require a homogeneously nanostructured substrate up to a millimeter scale. In principle conventional methods like photolithography or e-beam lithography fail to fabricate such a substrate. Photolithography does not reach the required resolution; e-beam lithography gives access to this resolution but since it is a serial writing method it is tedious to extend the nanopatterns to a millimeter scale.

For this reason we developed a new method called block copolymer micelle nano-lithography that uses the feature of self assembly to extend nanometer patterns to macroscopic length scales. The self assembly blocks consist of block copolymer micelles filled with gold nanoparticles. To obtain a mono-micellar film we dip the substrate into the micelle solution and pull it out with constant velocity. Because of evaporation the solvent toluene retracts and thereby forces a dense packing of the micelles on the substrate, leaving a regular, hexagonal pattern behind (see figure 1a) [3]. At this stage the gold nanodots are shielded by a polymer shell which can be removed in a second step by plasma treatment. Thereby plain gold dots are deposited onto the substrate. With this method we can precisely control the size of the gold nanoparticles (about 10nm) and also the spacing in the hexagonal pattern (by varying the polymer chain length) from 20 up to 100nm [4].

Subsequently, the homogenous nanopatterns are biofunctionalized by binding the RGD-sequence specifically to the gold nanoparticles whereas the plain substrate is passivated with poly ethylene glycol (PEG), mimicking an ECM with defined geometry. If a cell approaches such a substrate, only gold particles offering the RGD-sequence are possible anchor points for the integrins. In addition, because of steric means, it is expected that each gold particle can be occupied by only one integrin protein. Substrates with different spacings (28, 58, 73 and 85nm) are incubated with cells. After 24 hours we counted the number of spreaded cells per square millimeter. We find that the cells nicely adhere on 28 and 58 nm substrates but adhesion completely fails on 73 and 85nm spacings with a sharp transition at 73nm (see figure 1b) [5]. There are two possible reasons that may cause the adhesion failure: either the decrease in offered ligand density or the reduced total number of offered ligands. To distinguish between these two possibilities we create a new class of micro-nano structured interfaces by combining e-beam lithography with block copolymer micelle nanolithography [6, 7, 8]: Parts of the block copolymer micelle layer are exposed to an e-beam and get cross-linked. Thus by performing a lift off process with an appropriate solvent the illuminated regions remain on the substrate whereas the inviolate micelles are washed away. In this vein we fabricate substrates with separated squares (2μm x 2μm) of densely packed gold nanoparticles. The coarse grained density of offered ligands, however, is low because of the large separation of the high density regions. Cells plated on such substrates show spreading to a similar extent as cells plated on homogenous high density substrates. These experiments strongly suggest that indeed only the local concentration of offered ligand matters (and not the total amount of offered ligand). Thus we conclude that the integrins have to come into close contact to each other to get activated. This clustering then initiates focal adhesion formation. We performed these experiments with different cell types (3T3-Fibroblasts, REF52-Fibroblasts, MC3T3-Osteoblasts, B16-Melanocytes) and found 73nm to be a universal length scale for all cell types indicating that this spacing is a specific measure of the cluster-architecture itself.

Experiments have shown that mature focal adhesions (FA) undergo an anisotropic force-induced growth (along the force direction) when the actin stress is
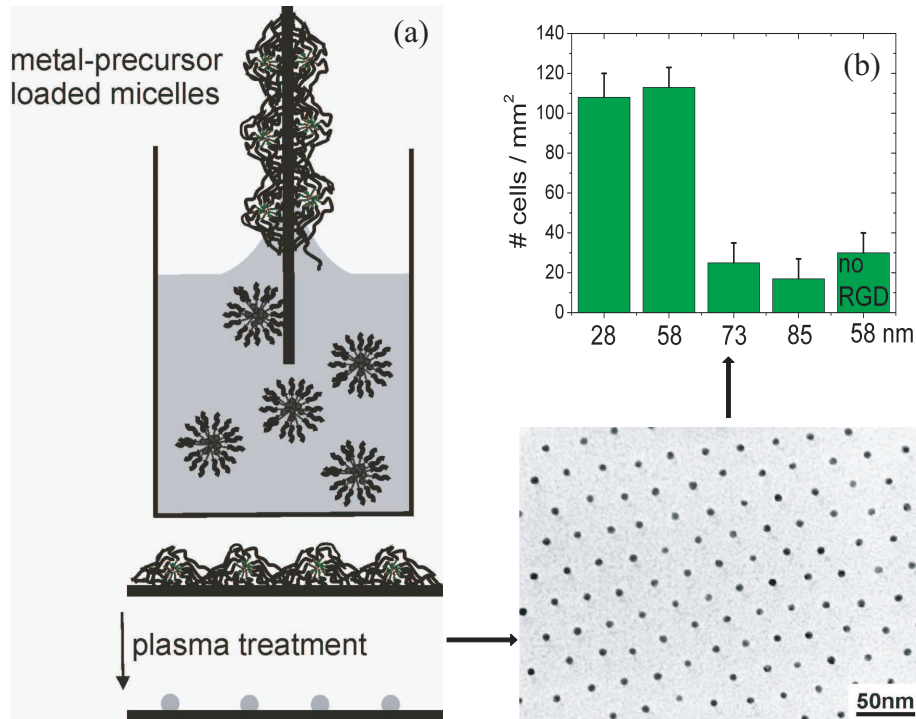
FIGURE 1. (a) Fabrication of nanopatterned surfaces. (b) Experimental results: Inhibition of cell spreading on 73nm patterns because of restricted integrin clustering [5].

increased [9]. The link between the force and the protein adsorption dynamics is the assumption that the force causes conformational changes of mechano-sensitive proteins located in the FA that in turn promote protein aggregation. Starting from these assumptions we first calculate the elastic deformations within the FA caused by the external stress. According to our model these local deformations determine the activation state of the mechano-sensitive proteins in the FA. When active these proteins can bind additional plaque proteins recruited from the cytosol and cause the adhesion to grow. We derive a partial differential equation that governs this change of plaque protein concentration within the focal adhesion in space and time:

$$(1) \qquad \frac{\partial \psi(x,t)}{\partial t} = \mu(\rho) + \epsilon\psi - c\psi^3 - g(\rho)\frac{\partial \psi}{\partial x} + B\frac{\partial^2 \psi}{\partial x^2},$$

where $\psi + 1/2$ is the plaque protein concentration ϵ, c, B are positive constants and μ, g are functions of the applied stress, denoted by ρ. For a physical description of the coefficients see [10]. Solving Eq.1 numerically we find that an initial step-like

front propagates into the low density domain (provided that the stress is in the appropriate regime) and reaches a steady state profile. By looking for moving front solutions $\psi(x, t) = \psi(x - vt)$ we determine the velocity at the front and at the back of the FA as a function of the applied stress. From this we can predict a variety of qualitative growth behavior for the FA in different force regimes including the anisotropic growth mentioned above, compare figure 8 in [10].

To quantitatively study this mechanosensitivity, we use microfabricated arrays of elastic polymer pillars coated with fibronectin to apply a lateral force to the cell. First we bring the pillar into contact with the cell. Because of the fibronectin the cell is recognizing the pillar and starts to reorganize its cytoskeleton. At this stage the intracellular tensions, built up by the actin-myosin contractility, are equilibrated over the whole cell. Now we displace the pillar relatively to the cell and thereby disturb the intracellular tension in such a way, that on one side of the cell, the forces on the FAs are increased whereas on the opposite side prestress is relieved and the forces on the FAs are decreased. Subsequently we expect a polarized behaviour of the cell: In the region where tension is increased the FAs are supposed to grow in size whereas in the region of decreased tension the FAs are expected to shrink. The resultant growth rates of FAs versus applied force are systematically measured and show the expected growth characteristics. By varying the external forces we are able to scan through the growth regimes predicted by our model [11].

REFERENCES

[1] B. Geiger, A. Bershadsky, R. Pankov and K.M. Yamada, *Transmembrane Extracellular Matrix - Cytoskeleton Crosstalk*, Nat. Rev. Mol. Cell Biol. **2** (2001), 793–805.
[2] J. Takagi, B.M. Petre, T. Walz and T.A. Springer, *Global Conformational Rearrangements in Integrin Extracellular Domains in Outside-In and Inside-Out Signaling*, Cell. **110** (2002), 599–611.
[3] J.P. Spatz, A. Roescher, S. Sheiko, G. rausch and M. Moeller, *Noble metal loaded block ionomers. Micelle organization, adsorption of free chains, and formation of thin films*, Advanced Materials **7**(8) (1995), 731–5.
[4] J.P. Spatz, A. Roescher and M. Moeller, *Gold nanoparticles in micellar poly(styrene)-b-poly(ethylene oxide) films. Size and interparticle distance control in monoparticulate films*, Advanced Materials **8**(4) (1996), 337–40.
[5] M. Arnold, A. Cavalcanti-Adam, R. Glass, J. Blummel, W. Eck, M. Kantlehner, H. Kessler and J.P. Spatz, *Activation of integrin function by nanopatterned adhesive interfaces*, Chem. Phys. Chem. **5** (2004), 383–388.
[6] R. Glass, M. Moeller and J.P. Spatz, *Block copolymer micelle nanolithography*, Nanotechnology **14**(10) (2003), 1153–1160.
[7] R. Glass, M. Arnold, J. Bluemmel, A. Kueller, M. Moeller and J.P. Spatz, *Micro-nanostructure interfaces fabricated by the use of inorganic block copolymer micellar monolayers as negative resist for electron-beam lithography*, Advanced Functional Materials **13**(7) (2003), 569–575.
[8] R. Glass, M. Arnold, E.A. Cavalcanti-Adam, J. Blummel, C. Haferkemper, C. Dodd and J.P. Spatz, *Block copolymer micelle nanolithography on non-conductive substrates*, New Journal of Physics **6** (2004), 101.

[9] D. Riveline, E. Zamir, N.Q. Balaban, U.S. Schwarz, T. Ishizaki, S. Narumiya, Z. Kam, B. Geiger and A.D. Bershadsky, *Focal contacts as mechanosensors: externally applied local mechanical force induces growth of focal contacts by an mDia1-dependent and ROCK independent mechanism*, J. Cell Biol. **153** (2001), 1175–1185.

[10] A. Besser and S.A. Safran, *Force-Induced Adsorption and Anisotropic Growth of Focal Adhesions*, Biophysical Journal **90**(10) (2006), 3469–3484.

[11] P. Heil et al. In preparation.

Aspects of modeling transport in small systems with a look at motor proteins

David Kinderlehrer

Diffusion-mediated transport is a phenomenon in which directed motion is achieved as a result of two opposing tendencies: diffusion, which spreads the particles uniformly through the medium, and transport, which concentrates the particles at some special sites. It is implicated in the operation of many molecular level systems. These include some liquid crystal and lipid bilayer systems, and, especially, the motor proteins responsible for eukaryotic cellular traffic. All of these systems are extremely complex and involve subtle interactions on widely varying scales. The chemical/mechanical transduction in motor proteins is, by contrast to many materials microstructure situations, quite distant from equilibrium. These bio-systems function in a dynamically metastable range. There is an enormous biological literature about this, [15] for a recent collection of reviews, and a considerable math-biology and biophysics literature, including [1],[2],[5],[13],[14].

Our approach is to look at a dissipation principle for such situations and its relationship to the Monge-Kantorovich mass transfer problem, eg. [16]. In effect, we begin with simple - but not too simple - assumptions of motion along a track followed by statistical assumptions which provide us an ensemble. The procedure permits us to establish consistent thermodynamical dissipation principles from which evolution equations follow. In a given instance, the dissipation principle identifies the thermodynamic free energy, the conformational changes that result, for example, from ATP hydrolysis reactions, and dissipation.

For illustration, suppose that our system admits n possible states governed by potentials $\psi_1, ..., \psi_n$ and populated by elements with densities $\rho_1, ..., \rho_n$, which are subject to conformational changes governed by a rate matrix $A = (a_{ij})$. Suppose it lives on the unit interval $\Omega = (0,1)$ and the potentials are periodic of period $\lambda = 1/N$. The dissipation principle we study is simply this: from a state $\rho^* = (\rho_1^*, ..., \rho_n^*)$, determine a successor state $\rho = (\rho_1, ..., \rho_n)$ by the minimization principle

$$\frac{1}{2\tau} \sum_{i=1,,n} d(\rho_i, (\rho^* P)_i)^2 + F(\rho) = \min$$

(1)

$$F(\rho) = \sum_{i=1,,n} \int_\Omega (\psi_i \rho_i + \sigma \rho_i \log \rho_i) dx$$

$$P = \mathbf{1} + \tau \mathbf{A}$$

Above, d denotes the Wasserstein (2) metric, σ is a diffusion constant, and τ is a relaxation time. We may easily identify F as the free energy of the system and the dissipation principle shows that the Wasserstein term represents dissipation. Conformational change is governed by changing $\rho^* \to \rho^* P$ prior to executing the move governed by the potentials. The minimum is taken over an appropriate set of nonnegative densities subject to

(2)
$$\rho_i \geqq 0, \quad \sum_{i=1,,n} \int_\Omega \rho_i = 1$$

Variational principles of this form with $n = 1$ have been known for some time, Jordan, Kinderlehrer [7], Otto [9], [10], Kinderlehrer and Walkington [8]. What may be less known is that (1) leads to a system, specifically,

(3)
$$\frac{\partial \rho}{\partial t} = \frac{\partial}{\partial x}(\sigma \frac{\partial \rho}{\partial x} + \rho \psi') + \rho A \; in \; \Omega$$

$$\sigma \frac{\partial \rho}{\partial x} + \rho \psi' = 0 \; on \; \partial\Omega$$

We then seek simple paradigms, analogous to coin toss, for transport and attempt to derive them from the dissipation principle or the differential equations. This will provide diagnostics for attempts at more detailed theories where more details of the transformation pathway are accomodated. At the simplest level of counting kinesin heads as ATP bound, ADP bound, or product bound or attached or detached from the microtuble, there are already $2^6 = 64$ combinatorial possibilities, of which (1) represents a 'most likely' choice. We are lead to investigate the conditions on interaction potentials and conformation change which lead to a not-very-simple demonstration of the paradigm. These involve asymmetry of the ψ_i within its period intervals and, second, locating the sites of conformational change. Considerations reminiscent of ergodicity for the probability matrix P in (1) play an interesting role.

A very interesting entropy-based proof on trend to stationarity is given by Perthame [12]. There are a number of fascinating examples related to the flashing rachet, perhaps a mechanism in KIF-1A transport, conventional kinesin, and even a gaming opportunity known as Parrondo's Paradox.

This is joint work with Michel Chipot, Stuart Hastings, David Heath, Michal Kowalczyk, and Bryce McLeod. Versions of papers, in particular, [3], [4], and [6],

are available at

http://www.math.cmu.edu/cna/publications.html

REFERENCES

[1] A. Ajdari and J. Prost, *Mouvement induit par un potentiel périodique de basse symétrie: dielectrophorese pulse*, C. R. Acad. Sci. Paris **315** (1992), 1653.

[2] R.D. Astumian, *Thermodynamics and kinetics of a Brownian motor*, Science **276** (1997), 917–922.

[3] M. Chipot, S. Hastings, and D. Kinderlehrer, *Transport in a molecular motor system* Math. Model. Numer. Anal. (M2AN) **38** (2004), 1011–1034.

[4] M. Chipot, D. Kinderlehrer and M. Kowalczyk, *A variational principle for molecular motors*, Meccanica **38** (2003), 505–518.

[5] C. Doering, B. Ermentrout and G. Oster, *Rotary DNA motors*, Biophys. J. **69** (1995), 2256–67.

[6] S. Hastings, D. Kinderlehrer and J.B. McLeod, *Diffusion mediated transport in multiple state systems* (submitted).

[7] R. Jordan, D. Kinderlehrer and F. Otto, *The variational formulation of the Fokker-Planck equation*, SIAM J. Math. Anal. Vol. **29** (1998), 1–17.

[8] D. Kinderlehrer and N. Walkington, *Approximation of parabolic equations based upon Wasserstein's variational principle*, Math. Model. Numer. Anal. (M2AN) **33** (1999), 837–852.

[9] F. Otto, *Dynamics of labyrinthine pattern formation: a mean field theory*, Arch. Rat. Mech. Anal. **141** (1998), 63–103.

[10] F. Otto, *The geometry of dissipative evolution equations: the porous medium equation*, Comm. PDE **26** (2001), 101–174.

[11] A. Parmeggiani, F. Jülicher, A. Ajdari and J. Prost, *Energy transduction of isothermal ratchets: generic aspects and specific examples close and far from equilibrium*, Phys. Rev. E, **60** (1999), 2127–2140.

[12] B. Perthame, *The general relative entropy principle – applications in Perron-Frobenius and Floquet theories and a parabolic system for biomotors*, Rendiconti Accademia Nazionale delle Scienze detta dei XL Memorie di Matematica e Applicazioni **122** (2006) vol. XXVIII fasc. 1.

[13] C.S. Peskin, B. Ermentrout and G.F. Oster, *The correlation ratchet: a novel mechanism for generating directed motion by ATP hydrolysis*, in Cell Mechanics and Cellular Engineering (V.C Mow et.al eds.), Springer, New York (1995).

[14] P. Reimann, *Brownian motors: noisy transport far from equilibrium*, Phys. Rep. **361** (2002), 57–265.

[15] M. Schliwa, ed, *Molecular Motors*, Wiley-VCH Verlag, Wennheim (2003).

[16] C. Villani, *Topics in optimal transportation*, AMS Graduate Studies in Mathematics vol. 58, Providence (2003).

Mathematical modeling of cell membrane organization, dynamics and trafficking

ANNE KENWORTHY

Cell membranes are organized in a bilayer structure, consisting of both protein and lipid components. A major question concerning membrane organization is whether these components are randomly distributed or instead form microdomains, spatially distinct regions of specialized protein and lipid composition. Among the

most widely studied, yet least well understood types of microdomains are a class of cholesterol-enriched domains termed lipid rafts. Lipid rafts have been postulated to participate in numerous cellular events ranging from cell signaling to membrane trafficking. A major challenge to understanding the mechanisms by which such domains function is the limited amount of structural information currently available about these domains. We have therefore employed biophysical approaches to probe the size, composition, and number of these domains present in cell membranes.

One such biophysical approach, fluorescence resonance energy transfer (FRET), is a method that can detect the distance between two fluorescently labeled molecules. We have used this technique to test the hypothesis that putative protein components of lipid rafts are distributed non-randomly in membranes, and in particular that they are enriched in domains that are sub-micron in dimensions [1, 2, 3]. FRET is sensitive to distances, yet we wish to discern underlying two-dimensional patterns of proteins. To address this mathematically underdetermined problem, we have used a Monte-Carlo based simulation of FRET in order to identify characteristic FRET signatures of different types of domains [4]. This approach has suggested a new experimental approach to the design of FRET measurements to determine the domain radius and inter-domain distance. We are currently extending these studies to consider effects of domain inter-connectedness and shape, as well as compare the predictions of several different models for lipid raft formation (partitioning, lipid shells, and actively maintained domains) which we will then test experimentally.

In a second line of study, we have examined the role lipid rafts play on the lateral diffusion of membrane proteins. Current models predict that association of proteins with lipid rafts should either slow protein diffusion or lead to the immobilization of raft-association proteins (Figure 1). To test this hypothesis, we have used a technique known as fluorescence recovery after photobleaching [5]. We found that the lateral mobility of a variety of proteins predicted to associate with lipid rafts based on biochemical criteria show little evidence for either immobile rafts or stable raft association, as predicted by qualitative models (Figure 1, models 1 and 2). However, we noted a ten-fold difference in the diffusion coefficient for the proteins studied. We are currently testing the source of this variation, which could either reflect dynamic partitioning of different proteins with lipid rafts (Figure 1, model 3) or other differences among these proteins (Figure 1, model 4), such as the size of the membrane-embedded region of the various proteins [6]. We are also interested in examining the possibility that these proteins exhibit anomalous diffusion, which could potentially provide some clues as to the mechanisms contributing to their differential diffusional mobilities.

References

[1] A.K. Kenworthy and M. Edidin, *Distribution of a glycosylphosphatidylinositol-anchored protein at the apical surface of MDCK cells examined at a resolution of $< 100\text{Å}$ using imaging fluorescence resonance energy transfer*, J. Cell Biol. **142** (1998), 69–84.
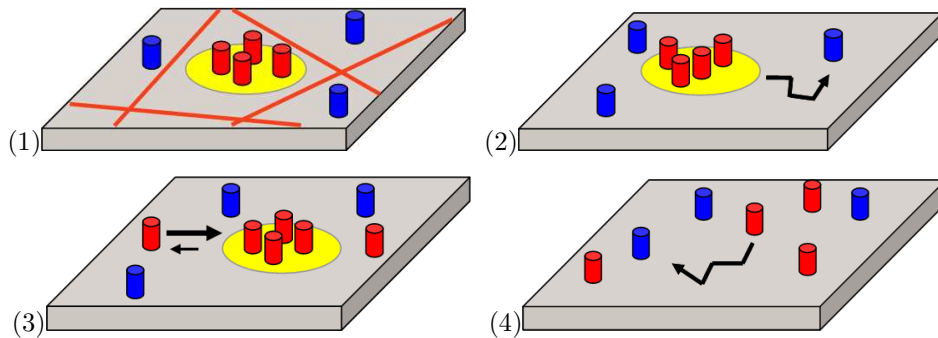
FIGURE 1. Models for how lipid rafts could influence the lateral diffusion of raft-associated membrane proteins. Lipid rafts are indicated by the yellow disks. The surrounding non-raft membrane is gray. Raft-preferring proteins are shown in red, and non-raft proteins in blue. (1) **Stable, immobile rafts.** Hypothetical barriers to lipid raft diffusion are depicted by the red lines. This model predicts that raft-associated proteins would be immobilized. (2) **Stable, mobile rafts.** Here, lateral diffusion is dominated by the diffusion of the raft rather than individual proteins. (3) **Dynamic partitioning of raft proteins.** Here, individual raft proteins could exhibit varying diffusional mobilities, reflecting a combination of their diffusion inside and outside of rafts. (4) **No rafts.** In the absence of rafts, the diffusion of individual proteins should be governed by both their structure (for example, lipid anchored versus transmembrane) and their interactions with other components of cell membranes (not shown). Reproduced from The Journal of Cell Biology, 2004, vol. 165 pp. 735-746 by copyright permission of The Rockefeller University Press.

[2] A.K. Kenworthy, N. Petranova and M. Edidin, *High-resolution FRET microscopy of cholera toxin B-subunit and GPI-anchored proteins in cell plasma membranes*, Mol. Biol. Cell **11** (2000), 1645–1655.

[3] A.K. Kenworthy, *Peering inside lipid rafts and caveolae*, Trends Biochem. Sci. **27** (2002), 435–438.

[4] M.A. Byrne, A.K. Kenworthy, *In silico characterization of resonance energy transfer for disk-shaped membrane domains*, (In preparation).

[5] A.K. Kenworthy, B.J. Nichols, C.L. Remmert, G.M. Hendrix, M. Kumar, J. Zimmerberg and J. Lippincott-Schwartz, *Dynamics of putative raft-associated proteins at the cell surface*, J. Cell Biol. **165** (2004), 735–46.

[6] Y. Gambin, R. Lopez-Esparza, M. Reffay, E. Sierecki, N.S. Gov, M. Genest, R.S. Hodges, and W. Urbach, *Lateral mobility of proteins in liquid membranes revisited*, Proc Natl Acad Sci USA (2006), vol. 103, pp. 2098–2102.

Modeling of cytoplasm motion and cell migration
Wolfgang Alt
(joint work with Esa Kuusela)

Interactive Motion of Actin Filaments. The movement and interaction of actin filaments as semi-flexible inextensible rods can be represented by the dynamics of a few nodes along each filament, interpolated by linear or cubic spline curves. Forces acting on any filament point are condensed to the nearest nodes and can consist of bending or friction forces, random or interaction forces, so that a system of stochastic ordinary differential equations for positions and velocities of all nodes arises. Resulting simulations reproduce the "flickering" behavior of single actin filaments with a mean directional persistence length of several μm. In the easiest case interactions between two filaments, e.g. via binding of cross-linking dimers as myosin, can be modeled by attractive forces between nodes of different filaments, provided their distance falls into a certain interaction range. More general, the stochastic interaction forces by transient binding and unbinding of cross-linkers can be lumped in a mean interaction kernel which, at least for straight rod segments, can be explicitly written in terms of interaction angle and distance. Resulting numerical analysis and simulations show partial alignment with deviations depending on the type of stochastic inputs (ongoing joint work with Dagmar Bär and Andreas Hilboll, Bonn).

Viscous Two-phase Flow Model for the Cytoplasm. The cytoplasmic actin-myosin system is embedded into an aqueous environment containing all kinds of monomers, oligomers and other regulating proteins and can thus biophysically be regarded as an "active fluid", namely a contractile, reactive and highly viscous two-phase fluid, mathematically modeled by a hyperbolic-elliptic system of mass and force balance equations (see Alt&Dembo 1999). In the case of negligible water viscosity, it essentially consists of the compressible Stokes equations for the actin polymer network with a hydrodynamic pressure due to drag flow between water and polymers, satisfying Darcy's law, and a "cubic like" pressure state function expressing dispersing and swelling pressures for low and high network concentrations, but contractile stresses for intermediate concentrations where myosin dimers can cross-link the network filaments.

Already in the simplest case of a fixed 1-dimensional domain with no-flux boundary conditions, the contractile flow model with simple linear assembly kinetics reveals a rich repertoire of different dynamical behavior as steady states, periodic solutions with repetitive waves as well as chaotic dynamics, see Fig. 1.

In a biological cell, or a cell fragment, this "active fluid" of actin-myosin polymers is surrounded by a plasma membrane, in which many kinds of proteins and receptors are more or less freely floating. The kinetic and dynamic interaction of actin filaments with such membrane proteins (e.g. integrins) determine the boundary conditions for velocities and pressures at the free or fixed parts of the
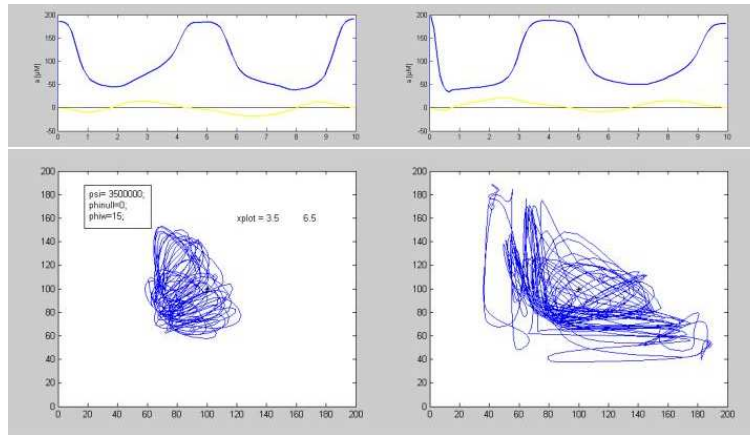
FIGURE 1. Simulation of the 1-d two-phase flow model with drag coefficient $phiw = 15$ induces a chaotically moving center of contracted F-actin in the middle region, performing different modes of spatial coupling between the two contraction-relaxation oscillators near the boundaries.

cell boundary. The latter is representing the boundary between lamellipodium and the cell body and there the network is sticking, but water can stream in or out depending on the given cell body pressure. At the free lamella tip boundary, normal velocity of F-actin could be less than or equal to the normal water and membrane velocity. The case of inequality means that the actin network is ruptured from the membrane, which then can be pushed forward by hydrodynamic or swelling pressures, while in the case of equality the actin network is locally attached to membrane proteins, whereby protrusion of the membrane can be withhold.

1-D and 2-D simultions reflect typical phenomena such as cell spreading, steady contraction patterns, cyclic protrusion-retraction activity of the leading lamella and periodic "ruffle" waves, all observed in experimental images of stationary or migrating tissue cells as, for example, keratinocytes (human epidermal cells), see Fig. 2.

1-D Model of Cell Adhesion and Migration. In order to model cell adhesion and migration, the one-dimensional cytoplasm flow model for a section through the leading lamella (or a corresponding cell fragment) described by the above-mentioned hyperbolic-elliptic transport system, is coupled to a four-state system for the kinetics of integrin receptors, which are either freely diffusing, or only bound to actin and then transported, or bound to the underlying substratum and then fixed; in case of additional binding to actin, the substratum experiences contractile or viscous shear forces applied by actin filaments in connection to so-called "focal adhesion complexes". The dissociation rate of these adhesive bonds is modeled to exponentially increase with increasing force. All the kinetic rates can be regulated
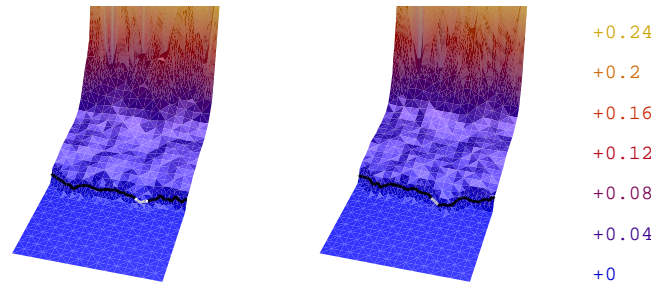
FIGURE 2. Shown are two consecutive plots of actin concentration in a lamellipodium model with free boundary at the lamella tip, performing irregular protrusions and re-tractions combined with the appearance of slight "ruffles". Regions of free boundary where membrain velocity equals F-actin velocity is drawn black.

by internal signalling molecules, which we assume to be constant for the considered time span of several minutes.
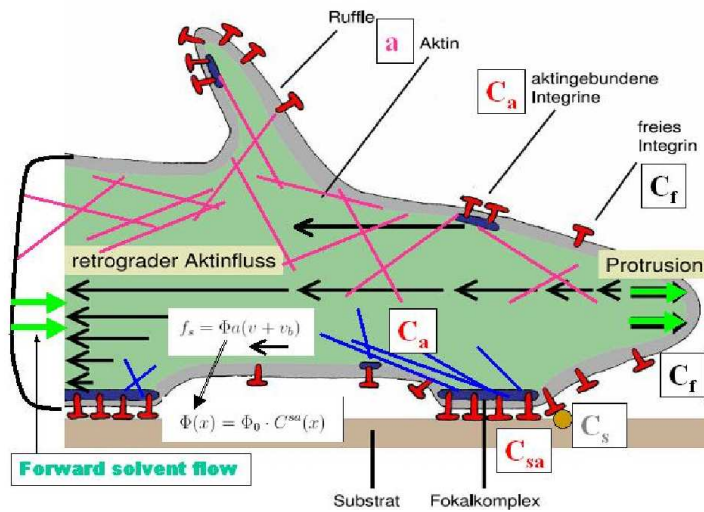
FIGURE 3. Schematic section through the tip of a protruding lamella with retrograde F-actin flow, denoted by v in moving lamella coordinates. If v_b denotes the lamella tip speed, then the force locally transmitted is proportionally to the local concentrations of F-actin (a), adhesion complexes (C_{sa}) and the retrograde flow speed $v + v_b$ relative to the fixed substratum.

The main result is spontaneous symmetry breaking and cell polarization (joint work with Christoph Möhl, now at FZ Jülich), and the corresponding model simulations reproduce experimental observations with cell lamella fragments. The migration speed can be shown to depend on various mechanical and chemical parameters as, for instance, the adhesive binding rate, which is proportional to the mean concentration of adhesion sites available at the substratum (experimentally realized by covering with differing concentrations of collagen or fibronectin filaments).

References

[1] W. Alt and M. Dembo, *Cytoplasm dynamics and cell motion: two-phase flow models*, Math. Biosciences **156** (1999), 207–228.

[2] W. Alt, *Nonlinear hyperbolic systems of generalized Navier-Stokes type for interactive motion in biology*. In: (S. Hildebrandt, H. Karcher eds.) "Geometric Analysis and Nonlinear Partial Differential Equations", Springer Verlag, Heidelberg et al. (2003), 431–461.

The role of chemotactic cell movement during development of the social amoebae Dictyostelium discoideum and gastrulation in the chick embryo

Cornelis J. Weijer

Development of multicellular organisms is critically dependent on a number of distinct cellular behaviours especially cell division, cell death, cell differentiation and cell movement. These processes all have to be precisely controlled in space and time. We investigate the molecular mechanisms by which cells signal each other during development and furthermore how cells detect these signals and translate this information into directed coordinated movement. We study these questions in two different experimental systems, the social amoebae *Dictyostelium discoideum*, a simple genetically tractable micro-organism showing a relatively simple starvation induced multicellular development, and during gastrulation in the chick embryo, a model system for early amniote (human) development.

In Dictyostelium starvation for food (bacteria) induces the aggregation of thousands of individual amoebae into a multi-cellular aggregate. During aggregation the cells differentiate into a number of distinct celltypes, which form a migrating slug that transforms into a fruiting body consisting of a stalk supporting a mass of spores. The chemotactic aggregation of the cells is controlled by propagating waves of cyclic-AMP emanating periodically from aggregation centres. These cAMP waves generally propagate as spiral waves from the aggregation centre outward and direct the periodic chemotactic movement of amoebae during the rising phase of the wave towards the aggregation centres. Cells move during the rising phase of the waves in the direction of the rising gradient and are refractory when the wave passes and the concentrations of cAMP are falling. Experiments show that also in the multicellular stages of development the migration of the cells

Propagating waves control Dictyostelium morphogenesis
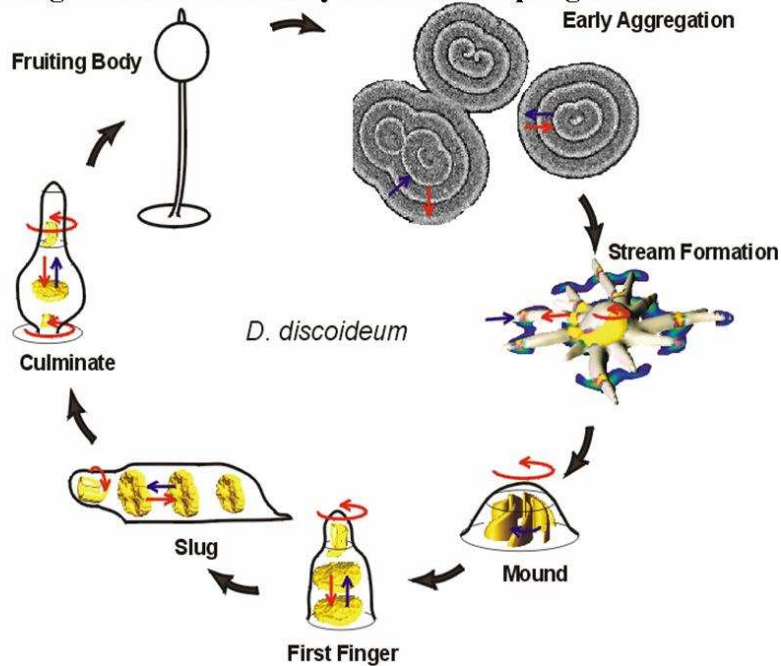
FIGURE 1. Spiral waves control cell movement during aggregation, stream formation, mound and slug formation, and migration. Red arrows indicate direction of wave propagation, blue arrows indicate direction of cell movement.

is guided by propagating waves of cAMP. Furthermore a combination of experimental data and analysis of mathematical models describing the dynamics of the interactions between wave propagation and chemotaxis, have shown that these two mechanisms, wave propagation and directed chemotactic movement in response to these waves, are sufficient to explain the principles of Dictyostelium morphogenesis. Detailed calculations have shown that the interactions between wave propagation and the resulting directed cell movement can explain the formation of aggregation streams and aggregation territories. All the cells in a given aggregation territory, aggregate into a hemispherical structure, the mound. The movement of the cells in the mound is still organised by propagating waves of cAMP, resulting in rotational movement of the cells in the mound. During aggregation cells start to differentiate into precursors of the stalks and the spore cells, the so called prestalk and prespore cells. The prestalk cells are able to develop more chemotactic movement force in response to the cAMP signals and as a result they are able to out-compete the prespore cells and move towards the source of the cAMP signal, the core of the spiral wave in the centre of the aggregate. Since only prestalk cells are able to relay the

cAMP signal, this separation of cell types results in a change of signal geometry from scroll waves (3D spirals) in the mound before cell sorting to twisted scroll waves and planar waves in the forming slug. This change in wave geometry results in formation and elongation of the slug and controls its migration (figure 1). This is one of the first cases where the morphogenesis of a multicellular organism can be understood at the level of rules for cell behaviour and signalling interactions between cells that control these cell behaviours [1].

We are now analysing the in-vivo spatio-temporal dynamics of the signaltransduction processes leading to polarised activity of the actin-myosin cytoskeleton, which is ultimately responsible for force generation and movement [2].

We have also started to investigate whether similar principles of signal propagation controlling chemotactic movement are involved in the development of higher organisms, especially amniotes. Our experiments have shown that chemotaxis also appears to play a critical role in the control of cell movement during early development in the chick embryo. A developmental stage where cell movements are very important is gastrulation. During gastrulation cells that will form the mesoderm and endoderm move into the embryo to take up their correct topographical position in the embryo. During gastrulation the induction of the nervous system takes place as well and defects in the control of cell movement during gastrulation cause some of the most severe congenital defects, such as spina- bifida and malformations of the brain and heart defects. In higher organisms (amniotes) gastrulation involves the formation of a structure known as the primitive streak. This develops from the posterior pole of the embryo and extends into an anterior direction during a process known as streak formation. Before gastrulation the embryo consists of two cell layers: the epiblast, the cells of which will give rise to the embryo proper, and the hypoblast which will mainly form extra-embryonic structures, such as part of the umbillical cord and the placenta in humans. During gastrulation epiblast cells move towards the primitive streak, where they undergo an epithelial to mesenchymal transition and delaminate to become individual mesenchymal cells. These single cells now move into the streak in the space between the epiblast and the hypoblast. There they migrate away to form the mesoderm and definitive endoderm. During this process the cells migrate over large distances and so far their detailed movement patterns have not been well described, nor is it known which signals control their movement.

As a first step in the analysis of this process we have tracked the migration of mesoderm cells during gastrulation over a period of 18 hours of development (Figure 2) [3]. We have shown that the movement of mesoderm cells is controlled by a combined action of chemo-attractants and repellents. Cells in the streak are instructed to migrate away from the place of invagination by a repellent made in the streak. We have identified this repellent as a member of the fibroblast growth factor family, FGF8. After the cells have migrated out, a process known as regression starts, in which the tip of the streak moves back towards the posterior pole in the embryo. During the process of regression the most anterior structures of the embryo start to form, first the head followed by more posterior structures such
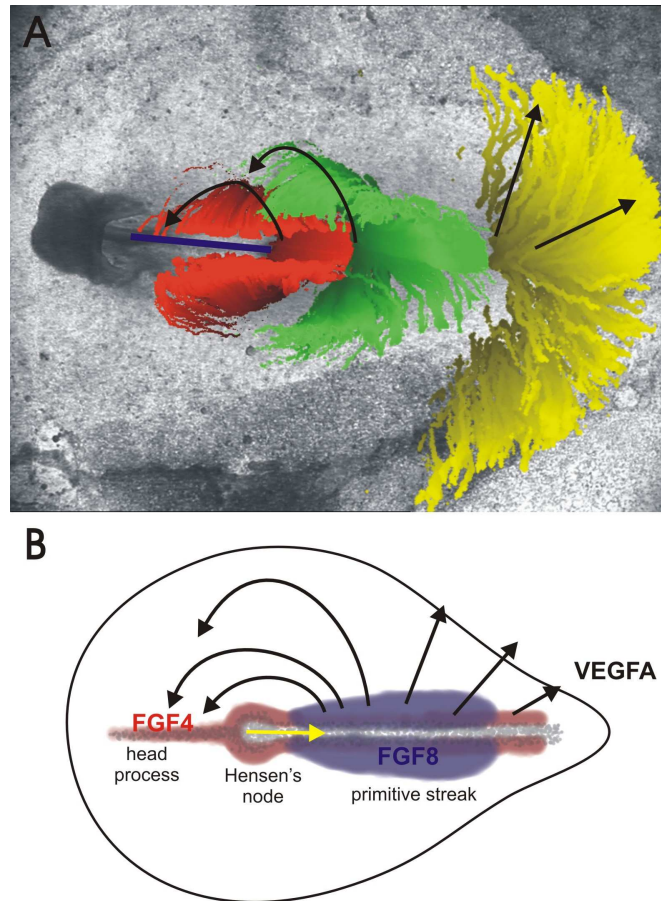
FIGURE 2. A: cell movement patterns observed during gastrulation. The node lays down the notochord (blue line) during regression. The mesoderm cells behind the node (red) migrate out of the streak and then move back towards the central midline to form the somites, the middle streak cells (green) form lateral plate mesoderm after their invagination, the posterior streak cells (yellow) form the haemopoietic cells (blood islands) after their migration from the streak. B: the migration away from the streak is controlled by a chemo-repellent action of FGF8 (blue) formed in the streak, while the anterior and middle streak cells are attracted back in towards the midline after regression of the node by FGF4 (red) made by the forming notochord.

as the somites. Somites are periodic structures formed of aggregates of mesoderm cells that will give rise to the segmented parts of the body, especially the muscles and the skeleton (ribs). The formation of somites requires a re-aggregation of the mesenchymal mesoderm cells that have migrated out of the streak. This process appears to be controlled by an attractant Fibroblast Growth Factor 4 (FGF4) produced by the notochord, the precursor of the vertebral column, that is laid down by the regressing tip of the streak and that attracts the cells in towards the central midline. FGF4 may also be involved in the control of the mesenchymal to epithelial transition during somite formation and compaction.

We now investigate how these FGF's are detected and result in directed attractive and repulsive cell movements of mesoderm cells. Furthermore we wish to understand how signalling and movement are integrated to result in the various stages including the formation of the primitive streak [4, 5].

References

[1] C.J. Weijer, *Dictyostelium morphogenesis*, Curr. Opin. Genet. Dev. **14** (2004), 392–398.

[2] M. Affolter and C.J. Weijer, *Signaling to Cytoskeletal Dynamics during Chemotaxis*, Dev. Cell **9** (2005), 19–34.

[3] X. Yang, D. Dormann et al., *Cell Movement Patterns during Gastrulation in the Chick Are Controlled by Positive and Negative Chemotaxis Mediated by FGF4 and FGF8*, Dev. Cell **3** (2002), 425–437.

[4] C. Cui, X. Yang et al., *Analysis of tissue flow patterns during primitive streak formation in the chick embryo*, Dev. Biol. **284** (2005), 37–47.

[5] D. Dormann and C.J. Weijer, *Visualizing cell movement*, EMBO J. (2006), in press.

Some mathematical problems in the modelization of Dd aggregation

Juan J. L. Velázquez

(joint work with G. Litcanu)

In this seminar I discuss two mathematical problems that arise in the study of the aggregation of the slime mold Dictyostelium discoideum. This organism lives during a large part of its life-cycle as an unicellular organism, but upon starvation conditions begins a process of aggregation that leads to the formation first of semi-spherical aggregates called mounds, and later some elongated cellular aggregates termed as slugs. In these aggregates the cells begin a process of differentiation that eventually leads to the formation of a fruiting body in the top where the sporae of the organism remain in a latent state until they find the right environmental conditions to develop again in the form of individual amobae.

The main idea of the talk is that there exist mathematical analysis techniques that allow to compute formulae from the models that eventually could be compared with experimental data.

During the process of aggregation the cells use a signalling mechanism based in the propagation of chemical waves of cAMP. Several models, based in different biochemical assumptions have been suggested in the literature (cf. [2], [4], [5], [6]).

In [3] we have analyzed, using singular perturbation methods, the models of Martiel-Goldbeter and Goldbeter-Segel. We analyzed first the Martiel-Goldbeter system, that reduces to a system of three differential equations for three variables γ, β, ρ_T that represent respectively the concentration of extracellular cAMP, intracellular cAMP and the fraction of occupied cell receptors. The differential equations that describe the evolution of these variables are then (cf. [4]):

$$
\begin{aligned}
\frac{\partial \rho_T}{\partial t} &= -f_1\left(\gamma\right)\rho_T + f_2\left(\gamma\right)\left(1 - \rho_T\right) \\
\frac{\partial \beta}{\partial t} &= q\sigma\phi\left(\rho_T, \gamma\right) - \left(k_i + k_t\right)\beta \\
\frac{\partial \gamma}{\partial t} &= \frac{k_t}{h}\beta - k_e\gamma + D\nabla^2\gamma
\end{aligned}
$$

(1)

$$
f_1\left(\gamma\right) = \frac{k_1 + k_2\gamma}{1 + \gamma} \ , \ f_2\left(\gamma\right) = \frac{k_1 L_1 + k_2 L_2 c\gamma}{1 + c\gamma}
$$

(2)
$$
\phi\left(\rho_T, \gamma\right) = \frac{\alpha\left(\lambda\theta + \epsilon Y^2\right)}{1 + \alpha\theta + \epsilon Y^2\left(1 + \alpha\right)} \ , \ Y = \frac{\rho_T\gamma}{1 + \gamma}
$$

where the numbers $D, k_1, k_2, L_1, L_2, c, \lambda, \ \theta, \alpha, \epsilon, k_i, k_t, k_e, q, h, \sigma$ are positive parameters. Using the numerical values of these parameters it is possible to rewrite this set of equations as a singular perturbation problem containing several small parameters. Using then the method of matched asymptotics we have checked that there exist travelling wave solutions of (1), (2) with the form of a pulse, and we have computed formulae for the wave speed, the width of the wave, and the concentrations of the different chemical species in the pulse.

In a second part of the talk, I discuss the main quantitative consequence of the Keller-Segel model. This model suggests that cellular concentrations might be described using continuous cell densities. It assumes also that the main effects that determine the number of cells that aggregate in a chemotaxis process are cell diffusion and chemotaxis attraction. The model might be written as:

$$
\begin{aligned}
\frac{\partial n}{\partial t} &= D_n\nabla^2 n - \chi\nabla\left(n\nabla c\right) \ , \ x \in IR^2 \ , \ t > 0 \\
\frac{\partial c}{\partial t} &= D_c\nabla^2 c + \alpha n - \beta c \ , \ x \in IR^2 \ , \ t > 0
\end{aligned}
$$

(3)

where the meaning of the parameters in the model is the following:

$$D_n = \text{Cell diffusivity}$$
$$D_c = \text{cAMP diffusivity}$$
$$\alpha = \text{Production rate of cAMP for cell.}$$
$$\chi = \text{Cell velocity induced for}$$
$$\text{unit of chemical gradient.}$$
$$\beta = \text{Degradation rate of chemical.}$$

There exists an extended mathematical theory describing the solutions of (3). In particular, it was derived by Childress (cf. [1]) that the number of cells aggregating in the "mound" is given by the following simple formula:

$$N_{cells} = \frac{8\pi D_c D_n}{\alpha \chi}.$$

References

[1] S. Childress, *Chemotactic collapse in two dimensions*, Modelling of Patterns in Space and Time, Lecture Notes in Biomath. **55**, Springer-Verlag, Berlin, (1984), 61–68.

[2] A. Goldbeter and L.A. Segel, *Unified mechanism for relay and oscillation of cyclic AMP in Dictyostelium discoideum*, Proc. Natl. Acad. Sci. USA **74** (1977), 1543–1547.

[3] G. Litcanu and J.J.L. Velázquez, Journal of Mathematical Biology **52** (2006), 682–718.

[4] J.L. Martiel and A. Goldbeter, *A model based on receptor desensitization for cyclic AMP signaling in Dictyostelium cells*, Biophys. J. **52** (1997), 807–828.

[5] P.B. Monk and H.G. Othmer, *Cyclic AMP oscillations in suspension of Dictyostelium discoideum*, Phil. Trans. R. Soc. Lond. **323** (1989), 185–224.

[6] Y. Tang and H.G. Othmer, *Excitation, oscillations and wave propagation in a G-protein-based model of signal transduction in Dictyostelium discoideum*, Phil. Trans. R. Soc. Lond. B **349** (1995), 179–195.

Macroscopic Taxis Equations from Cell-based Models

Hans G. Othmer

(joint work with Radek Erban)

Cell movement is an essential process at various stages in the life cycle of most organisms. Motile organisms sense their environment and can respond to it either by directed movement toward or away from a signal, which is called *taxis*, or by changing their speed of movement and/or frequency of turning, which is called *kinesis*, but for simplicity we denote both as taxis. Let Ω be a compact subset of $\mathbb{R}^N$ with smooth boundary. The classical Patlak-Keller-Segel chemotaxis equations, which govern the evolution of the macroscopic "particle" density n and the

"signal" density S, are

(1)
$$\frac{\partial n}{\partial t} = \nabla \cdot (\nabla n - n\chi \nabla S)$$

$$\frac{\partial S}{\partial t} = D\Delta S + f(n, S)$$

in Ω, with homogeneous Neumann data on the boundary. Here χ is the chemo-
tactic sensitivity coefficient. These equations have been studied intensively over
the last thirty years, and a great deal is known about the existence and unique-
ness of solutions for specific forms of χ and f [4]. However, except in examples
described later, little is known about how an individual-based description of signal
transduction and movement translates into the chemotactic sensitivity. Until re-
cently these coefficients were either simply postulated or derived from experimental
population-level statistics of movement.

   Many bacteria, such as *Escherichia coli* and *Proteus mirabilis*, use a "run-and-
tumble" strategy for movement, and in this case χ can be expressed in terms of
microscopic properties of individual cells. This case is treated in detail in [1, 2],
where we describe the movement of cells using a velocity-jump process [5], and
incorporate internal state variables of individual cells into the governing transport
equation. Thus suppose that the internal variables $\mathbf{y} \in Y \subset \mathbb{R}^m$ involved in signal
transduction and control of movement evolve according the equations

$$\frac{d\mathbf{y}}{dt} = \mathbf{f}(\mathbf{y}, \hat{S})$$

where $\hat{S}$ is some functional of the external signal and $\mathbf{f}(\cdot, \hat{S}) : Y \to \mathbb{R}^m$. Inclusion
of internal state variables in the velocity-jump process leads to the equation

(2) $$\frac{\partial p}{\partial t} + \nabla_{\mathbf{x}} \cdot \mathbf{v}p + \nabla_{\mathbf{y}} \cdot \mathbf{f}p = -\lambda(\mathbf{y})p + \int_V \lambda(\mathbf{y})T(\mathbf{v}, \mathbf{v}', \mathbf{y})p(\mathbf{x}, \mathbf{v}', \mathbf{y}, t)d\mathbf{v}'$$

where $p(\mathbf{x}, \mathbf{v}, \mathbf{y}, t)$ is the density of cells with internal state $\mathbf{y}$ at position $\mathbf{x}$, moving
with velocity $\mathbf{v} \in V \subset \mathbb{R}^N$ at time $t \geq 0$. Here we assume that the random
velocity changes are the result of a Poisson process of intensity $\lambda(\mathbf{y})$, and the kernel
$T(\mathbf{v}, \mathbf{v}', \mathbf{y})$ gives the probability of a change in velocity from $\mathbf{v}'$ to $\mathbf{v}$, given that a
reorientation occurs. The kernel T is non-negative and satisfies the normalization
condition $\int_V T(\mathbf{v}, \mathbf{v}', \mathbf{y})d\mathbf{v} = 1$. To connect this with the chemotaxis equation (1),
one has to derive an evolution equation for the macroscopic density

(3) $$n(\mathbf{x}, t) = \int_Y \int_V p(\mathbf{x}, \mathbf{v}, \mathbf{y}, t)d\mathbf{v}d\mathbf{y}$$

of individuals and formulate the evolution equation for the extracellular signal.
This has been carried out in detail for a simplified description of the internal
dynamics where $\mathbf{y} = (y_1, y_2)^T$ evolves according to

$$\frac{dy_1}{d\tau} = \frac{g(S(\tau)) - (y_1 + y_2)}{\tau_e}, \qquad \frac{dy_2}{d\tau} = \frac{g(S(\tau)) - y_2}{\tau_a}, \qquad \text{and} \qquad \lambda(\mathbf{y}) = \lambda_0 - by_1.$$

Here the first equation captures the rapidly-varying excitation step, whereas the second reflects the slower adaptation step. Clearly y_1 adapts perfectly to any signal, and thus it is used to modulate the turning rate as indicated. The reduction of (2) to the form (1) is done by an asymptotic analysis on suitable space and time scales, with the result that n evolves according to

$$\frac{\partial n}{\partial t} = \nabla \cdot \left(\frac{s^2}{N\lambda_0} \nabla n - n \cdot g'(S(\mathbf{x})) \frac{bs^2 \tau_a}{N\lambda_0(1 + \lambda_0 \tau_a)(1 + \lambda_0 \tau_e)} \nabla S \right)$$

where S is a time-independent signal field. Therefore the chemotactic sensitivity is given by

$$\chi = g'(S(\mathbf{x})) \frac{bs^2 \tau_a}{N\lambda_0(1 + \lambda_0 \tau_a)(1 + \lambda_0 \tau_e)}.$$

This incorporates the microscopic cell speed s, the sensitivity of the turning rate to the internal variable y_1, and the excitation and adaptation time scales τ_e and τ_a; for details of the derivation see [2].

A fundamental assumption in the use of velocity-jump processes to describe cell motion is that the jumps are instantaneous, and therefore the forces are Dirac distributions. This approximates the case in which very large forces act over very short time intervals, and even if one incorporates a resting or tumbling phase, as was done in [6, 1], the macroscopic description of motion is unchanged. This is appropriate for the analysis of bacterial motion (and other systems that use a "run-and-tumble" strategy), as summarized above, since there is no evidence that the signal affects the force generation mechanism itself.

However, the situation is very different when analyzing the movement of crawling cells such as leukocytes or fibroblasts, for here the control of the force-generation machinery is an essential component of the response. Therefore it is necessary to incorporate the force-generation machinery as part of the internal state, and as a first step we condense this all into a description of how the force exerted by a cell on its surroundings depends on the external signal. We denote the internal state by $\mathbf{y} \in \mathbb{Y}$, and the force per unit mass on the centroid of a cell by $\mathcal{F}(\mathbf{x}, \mathbf{v}, \mathbf{y})$. Here $\mathbb{Y}$ is a suitable, in general infinite-dimensional, Banach space. The internal state and velocity now evolve according to

$$(4) \qquad \frac{d\mathbf{y}}{dt} = \mathcal{G}(\mathbf{y}, S), \qquad \frac{d\mathbf{v}}{dt} = \mathcal{F}(\mathbf{x}, \mathbf{v}, \mathbf{y}).$$

Here $\mathcal{G} : \mathbb{Y} \times \mathbb{S} \to \mathbb{Y}$ is a mapping between Banach spaces and $\mathcal{F} : \mathbb{R}^N \times \mathbb{R}^N \times \mathbb{Y} \to \mathbb{R}^N$ where $N = 1, 2$, or 3 is the dimension of the physical space. This generality is needed because the internal state $\mathbf{y}$ can include quantities that depend on the location in the cell or on the membrane, and which may, for example, satisfy a reaction-diffusion equation or another evolution equation.

The cell is therefore described by the position and velocity of its centroid, and the internal state $\mathbf{y} \in \mathbb{Y}$. In some cases there is a projection $\mathcal{P} : \mathbb{Y} \to \mathbb{Z} \subset \mathbb{Y}$ from $\mathbb{Y}$ onto a suitable finite-dimensional subspace $\mathbb{Z}$, obtained for example by considering the first few modes in a suitable basis for $\mathbb{Y}$, such that

$$\mathcal{P}(\mathcal{G}(\mathbf{y}, S)) = \mathbf{G}(\mathbf{z}, S) \quad \text{and} \quad \mathcal{F}(\mathbf{x}, \mathbf{v}, \mathbf{y}) = \mathbf{F}(\mathbf{x}, \mathbf{v}, \mathbf{z}), \quad \text{where} \quad \mathbf{z} \equiv \mathcal{P}\mathbf{y}.$$

Here $\mathbf{G}(\cdot, S) : \mathbb{Z} \to \mathbb{Z}$ and $\mathbf{F}(\cdot, \cdot, \cdot) : \mathbb{R}^N \times \mathbb{R}^N \times \mathbb{Z} \to \mathbb{R}^N$ are mappings between finite-dimensional spaces. The first equality defines the function $\mathbf{G}$, whereas $\mathbf{F}$ is explicitly given by the second equality when the reduction is possible. Given a suitable choice of the projection $\mathcal{P}$, one can reduce the infinite-dimensional system (4) to the set of ordinary differential equations for the evolution of the internal state of individual cells.

$$(5) \qquad \frac{\mathrm{d}\mathbf{z}}{\mathrm{d}t} = \mathbf{G}(\mathbf{z}, S) \qquad \frac{\mathrm{d}\mathbf{v}}{\mathrm{d}t} = \mathbf{F}(\mathbf{x}, \mathbf{v}, \mathbf{z})$$

The transport equation (2) can now be written in the form

$$(6) \quad \frac{\partial p}{\partial t} + \nabla_{\mathbf{x}} \cdot \mathbf{v}p + \nabla_{\mathbf{v}} \cdot \mathbf{F}p + \nabla_{\mathbf{z}} \cdot \mathbf{G}p = -\lambda(\mathbf{z})p + \int_V \lambda(\mathbf{z})T(\mathbf{v}, \mathbf{v}', \mathbf{z})p(\mathbf{x}, \mathbf{v}', \mathbf{z}, t)\mathrm{d}\mathbf{v}'.$$

where here the right-hand side accounts for small random fluctuations of speed and direction.

In [3] we develop an infinite-dimensional model of the form (4) for a single cell and show that it can be reduced to a finite-dimensional version as given by (5). We show that the model for cell movement captures the essential features of movement in response to traveling waves of chemoattractant. Asymptotic analysis of the transport equation (6) then leads to a system of macroscopic hyperbolic equations, but it is not known if that system can in turn be reduced to (1). Details are given in [3].

REFERENCES

[1] R. Erban and H. Othmer, *From individual to collective behaviour in bacterial chemotaxis*, SIAM Journal on Applied Mathematics **65** (2004), no. 2, 361–391.
[2] ———, *From signal transduction to spatial pattern formation in* E. coli*: A paradigm for multi-scale modeling in biology*, Multiscale Modeling and Simulation **3** (2005), no. 2, 362–394.
[3] Radek Erban and Hans G. Othmer, *Taxis equations for amoeboid cells*, Preprint, 2006.
[4] D. Horstmann, *From 1970 until present: the Keller-Segel model in chemotaxis and its consequences I*, Jahresbericht der DMV **105** (2003), no. 3, 103–165.
[5] H. Othmer, S. Dunbar and W. Alt, *Models of dispersal in biological systems*, Journal of Mathematical Biology **26** (1988), 263–298.
[6] H. Othmer and T. Hillen, *The diffusion limit of transport equations 2: Chemotaxis equations*, SIAM Journal on Applied Mathematics **62** (2002), 1222–1250.

Bacterial pattern formation, a poorly understood phenomenon controlled by a complex interplay of chemistry, fluid mechanics and genetics: can a mathematical treatment simplify the analysis?

SIMONE J. SÉROR AND I. BARRY HOLLAND

Bacterial cells (rod shaped, 1 μ by 3-6 μ) can form large (approximately 50 sq/cm^2), intricately branched patterns, on a nutrient agar gel-like surface within a few hours. This involves a rapid mass migration over the surface from a central inoculation spot, in a process known as swarming. This process, ultimately producing billions of cells through growth and division, allows the bacteria to occupy a large surface territory. Swarming proceeds through a series of specific stages, including periods of aggregation of the cells into extended columns (dendrites). These dendrites grow and branch frequently as the swarm community expands, producing a pseudo-fractal formation. We have now documented the stages in this process in great detail, both micro- and macroscopically, for the soil bacterium and model laboratory organism, *B. subtilis* [1, 2, 3].

Swarming is dependent upon the presence of the long bacterial flagellum, normally used for propulsion (swimming), although the precise role in swarming is unclear. However, swarming also requires the production and release from the bacteria of a chemical, a small peptide, surfactin, that spreads ahead of the advancing swarm front [2]. Surfactin dramatically modifies the fluid mechanics of the surface water film on the agar, with effects that include an increased depth of this film at the swarm front. This may allow the cells to deploy more easily their flagella in some way.

The production of surfactin is controlled by a complex system of intercellular chemical signals generated by the bacteria. This is controlled by several genes, that induce the necessary number of cells to produce surfactin, *via* a quorum sensing mechanism. These signalling or communication systems mobilize the bacteria, in as yet poorly understood way, to behave cooperatively and in unison to achieve the observed coordinated swarming migration.

Thus, from our knowledge so far, a picture emerges of the swarming process as a complex interplay between chemical, physical and genetical elements. On the other hand, bacterial swarming does not appear to be driven by nutrient limitation. Indeed, the resulting pattern formation cannot be explained by existing theories, based on diffusion limited aggregation or *classical* chemotaxis towards nutrients. We suggest that mathematical modelling and simulations, based on relevant key parameters obtained from experimental measurements, can be successfully applied to this phenomenon. Currently, we are trying therefore to measure with precision over time, the number and speed of migration of cells, and the rate of diffusion and concentration of surfactin *in situ*. Initially, we hope to produce a mathematical model, based on a non-classical chemotaxis mechanism, that satisfactorily mimics the process. However, we hope ultimately this approach will lead to predictions that will rationalize the design of further experiments to elucidate more precisely
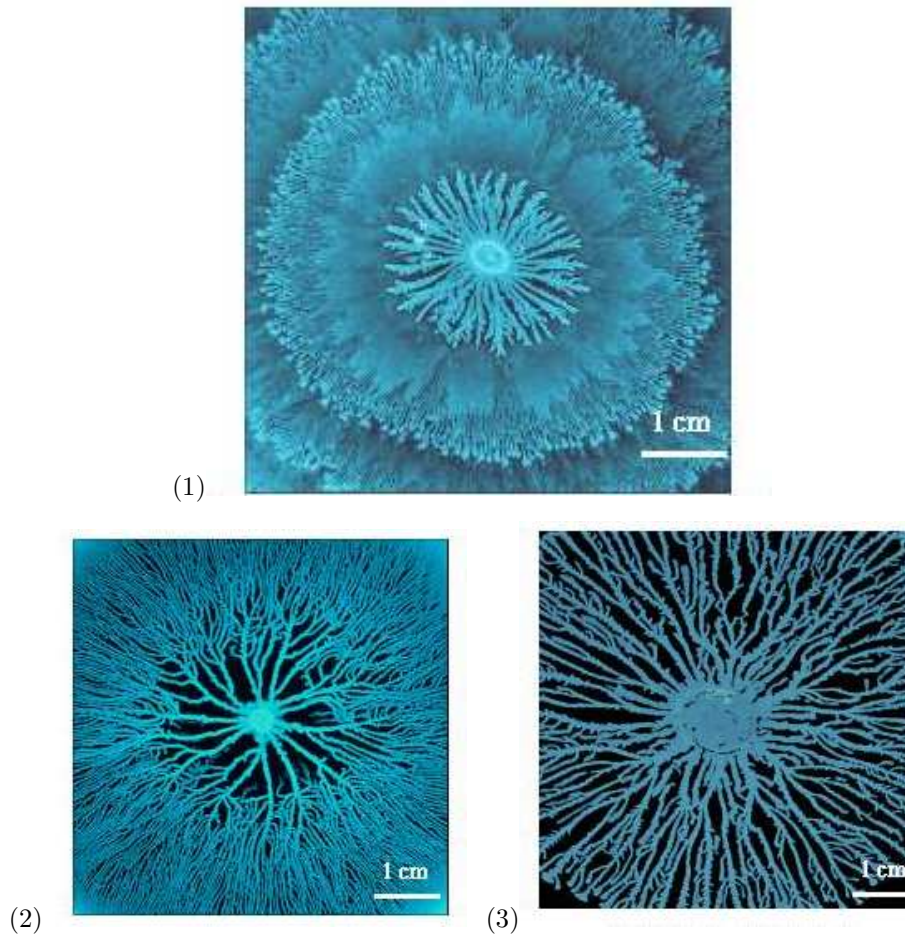
FIGURE 1. (1) Wild type swarming pattern (successive waves) shown in upper panel; (2,3) different patterns generated by two mutants in lower panels.

the contribution and mechanism of action of the different physico-chemical and genetic factors involved.

REFERENCES

[1] D. Julkowska, M. Obuchowski, I.B. Holland and S.J. Séror, *Branched swarming patterns on a synthetic medium formed by wild type Bacillus subtilis strain 3610: detection of different cellular morphologies and constellations of cells as the complex architecture develops*, Microbiology **150** (2004), 1839–1849.

[2] D. Julkowska, M. Obuchowski, I.B. Holland and S.J. Séror, *Comparative Analysis of the Development of Swarming Communities of Bacillus subtilis 168 and a Natural Wild Type: Critical Effects of Surfactin and the Composition of the Medium*, J. Bacteriol. **187** (2005), 65–76.

[3] I.B. Holland, D. Julkowska, K. Hamze and S.J. Séror, MicrobiologyToday (Quarterly Review of the Society General Microbiology, UK) **33**, 68–70.

Modelling populations of swimming micro-organisms

Timothy J. Pedley

(joint work with Takuji Ishikawa)

Bioconvection patterns are observed in shallow suspensions of randomly, but on average upwardly, swimming micro-organisms which are a little denser than water. The basic mechanism is analogous to that of Rayleigh-Benard convection, in which an overturning instability develops when the upper regions of fluid become denser than the lower regions. The reason for the upswimming however depends on the species of micro-organism: certain biflagellate algae are bottom-heavy, and therefore experience a gravitational torque when they are not vertical; certain oxytactic bacteria swim up oxygen gradients that they generate by their consumption of oxygen. Rational continuum models can be formulated and analysed in each of these cases, as long as the cell volume fraction n is low enough for hydrodynamic or other cell-cell interactions to be neglected ($n \leq 0.1\%$). The key mathematical step is the calculation of the probability density function for the cells' swimming velocity from a suitable Fokker-Planck equation, when that is justifiable. Both examples will be discussed from this point of view.

Another sort of pattern-formation ("whorls and jets") is observed in very concentrated, very shallow (effectively two-dimensional) cultures of swimming bacteria on agar plates. Something similar is seen in three dimensions, for example at the edge of a drop resting on a horizontal plate (see [1]). In both examples cell-cell interactions are crucial, but it is not clear how to derive an appropriate macroscopic model that is consistent with the laws of mechanics at the cellular level. A recent attempt [2] succeeds in generating 2D patterns on the correct scale, but appears not to be rationally justified.

Here we examine the deterministic swimming of model organisms which interact hydrodynamically but do not exhibit intrinsic randomness except in their initial positions and orientations. A micro-organism is modelled as a squirming, inertia-free sphere with prescribed tangential surface velocity. Pairwise interactions have been computed using the boundary element method, supplemented by lubrication theory, and the results stored in a database. The movement of many identical squirmers is computed by the Stokesian Dynamics method, with the help of the database (the restriction to pairwise interactions requires that the suspension be semi-dilute, with particle volume fraction less than about 0.1). It is found that in three dimensions the spreading of the squirmers is correctly described as a diffusive process sufficiently long after the motion is initiated, although all cell movements

are deterministic. The effective translational and rotational diffusivities depend strongly on volume fraction and mode of squirming. However, in two dimensions there is a definite tendency towards aggregation, again entirely as a consequence of the hydrodynamic interactions. Bottom-heavy squirmers, which tend to swim upwards, additionally show a tendency to form horizontal stripes in two dimensions, the stripes having an internal crystalline structure that has not yet been explained theoretically.

<div align="center">REFERENCES</div>

[1] C. Dombrowski et al, *Self-Concentration and Large-Scale Coherence in Bacterial Dynamics*, Phys. Rev. Lett. **93** (2004), 98103.
[2] J. Lega and T. Passot, *Hydrodynamics of bacterial colonies: A model*, Phys. Rev. E **67** (2003), 031906.

Integrative Mathematical Biology of Cancer Invasion

ALEXANDER R. A. ANDERSON, VITO QUARANTA

Cancer is a complex, multiscale process, in which genetic mutations occurring at a subcellular level manifest themselves as functional changes at the cellular and tissue scale. Existing models of solid tumour growth tend to focus on a single spatial scale, but often ignore the importance of the tumour microenvironment and lack clinical relevance. The importance of tumour cell/microenvironment interactions is currently of great interest to the biological community. In particular, both the immediate microenvironment (cell-cell or cell-matrix interactions) and the extended microenvironment (e.g. vascular bed) are thought to play crucial roles in both tumour progression and suppression.

In this joint presentation we will try to highlight the importance of multiscale mathematical models and the evolutionary implications of tumour growth in either harsh or mild microenvironmental conditions. We will present a hybrid multiscale mathematical model of the invasion of healthy tissue by a solid tumour and examine how changes in cell phenotypic attributes (e.g. p53 mutation, cell-cell adhesion, invasiveness) affect both tumour morpholgy and genetic makeup [4]. In particular we consider early vascular growth, just after angiogenesis has occurred and examine how the geometry of the growing tumour is affected by tumour cell heterogeneity caused by genetic mutations. As the tumour grows mutations occur leading to a heterogeneous tumour cell population with some cells having a greater ability to migrate, proliferate or degrade the surrounding tissue. All of these cell properties are closely controlled by cell-cell and cell-matrix interactions and as such the physical geometry of the whole tumour will be dependent on these individual cell interactions.

The hybrid discrete-continuum model [3] focuses on four key variables implicated in the invasion process: tumour cells, host tissue (extracellular matrix), matrix-degradative enzymes and oxygen. The model is considered to be hybrid since the latter 3 variables are continuous (i.e. concentrations) and the tumour

cells are discrete (i.e. individuals). Since the cells are considered as individuals we can assign each cell an individual life-cycle flow chart that takes into account both cell phenotype and microenvironmental influences. Its components include both basic metabolic processes, such as proliferation and oxygen consumption rates, as well as motility-related ones, such as the propensity to undergo haptotaxis and engage in cell-cell adhesion. The life-cycle flow chart is the core engine of the hybrid model, and provides a natural link between mathematics and biological experimentation. This is because, in the model as in reality, each cell behaves on its own, based on a phenotype determined both by genetic make-up and microenvironmental interactions.

Since the ability to assign a phenotype to each individual cell is a fundamental property of our hybrid discrete-continuum approach we shall present results from two separate algorithms for phenotype assignment: linear and random. In the linear scheme cells can unidirectionally mutate along a linear pathway of four increasingly aggressive phenotypes. For the random algorithm cells mutate without restriction to one of 100 predefined phenotypes. These phenotypes are initially generated by randomly selecting trait values with the same upper and lower bounds as the linear mutation scheme.

We shall examine how individual-based cell interactions (with one another and the microenvironment) can affect the tumour morphology and discuss which of these interactions is perhaps most crucial in influencing the tumour's final structure. We will also discuss the evolutionary influence that the microenvironment has upon the tumour's genetic makeup by considering growth in both mild and harsh environments. This link can be tested experimentally both in vitro, ex vivo and in vivo. We will discuss types of experimentation that are possible within the context of current technology.

Computational simulations of our model show that harsh conditions in the tumour microenvironment (e.g., heterogeneous extracellular matrix or hypoxia) result in tumours that grow with irregular, fingering margins (figure 1) and that consist of a few aggressive cancer cell clones which dominate. In contrast, in mild microenvironment conditions (e.g., normoxia or homogeneous ECM concentrations) such aggressive clones do not invade nor dominate. The tumour grows with smooth margins (no fingering) and is comprised of a larger number of mixed phenotypes i.e. less aggressive phenotypes in addition to more aggressive ones. These simulation outcomes clearly show that it is possible to identify the physical selective forces that operate in the microenvironment, and the effect they may have on tumour growth. Experimental validation will provide a quantitative foundation for the model. In addition, the simulations establish a clear link between selected phenotypes and emergent properties of the tumour mass, i.e. invasive (fingering margins) or non-invasive (smooth margins).

The selective forces of the microenvironment ultimately act upon genes or their products, though they effectively select cell phenotypes. Therefore, it is easy to see how the model spans biological scales, from molecules (genes and their products) to tissue (tumour mass). In fact, the hybrid discrete-continuum model focuses
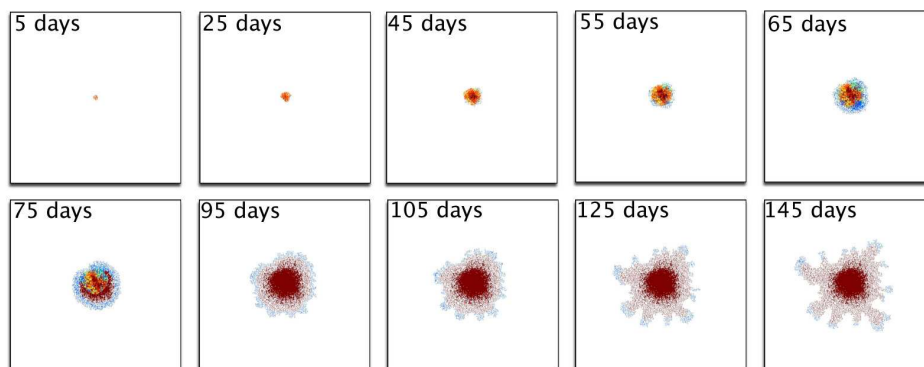
FIGURE 1. Heterogeneous tumour simulation results, showing a
tumour growing over a period of 21 weeks. Starting initially with
only 50 cells and ending with over 200,000 cells. Colouration
signifies the aggressiveness of the tumour cells, blue being the
most aggressive and orange the least, with yellow/green being
intermediate and brown represents dead cells.

on the micro-scale (individual cell) level to produce computational simulations
of tumour at the tissue scale. This technique, developed in previous models of
angiogenesis [2], and nematode movement [1] is intrinsically multiscale and can
easily incorporate a range of scales i.e. genetic, sub-cellular, cellular and tissue.

REFERENCES

[1] A.R.A. Anderson, B.D. Sleeman, I.M. Young and B.S. Griffiths, *Nematode movement along
    a chemical gradient in a structurally heterogeneous environment: II. Theory*, Fundam. appl.
    Nematol. **20** (1997), 165–172.
[2] A.R.A. Anderson and M.A.J. Chaplain, *Continuous and Discrete Mathematical Models of
    Tumour-Induced Angiogenesis Angiogenesis*, Bull. Math. Biol. **60** (1998), 857–899.
[3] A.R.A. Anderson, *A Hybrid Discrete-Continuum Technique for Individual Based Migration
    Models*, in Polymer and Cell Dynamics, eds. W. Alt, M. Chaplain, M. Griebel, J. Lenz,
    Birkhäuser (2003).
[4] A.R.A. Anderson, *A hybrid mathematical model of solid tumour invasion: The importance
    of cell adhesion*, IMA Math. App. Med. Biol. **22** (2005), 163–186.

Post-transplantation Dynamics of the Immune Response to Chronic Myelogenous Leukemia

Doron Levy

(joint work with Rob DeConde, Peter Kim, Peter Lee)

Chronic myelogenous leukemia (CML) is a blood cancer with a common acquired genetic defect resulting in the overproduction of malformed white blood cells. It constitutes nearly 20% of all leukemias, affecting roughly 1 in 100,000 people [15]. Prior to the recent introduction of the drug Gleevec (imatinib or STI571), the life expectancy of CML patients was about 4 years, with only 10% of all patients living beyond 8 years [3]. While these statistics are changing for the better with this new therapy, the requisite large-scale clinical studies have not yet been completed [14]. Gleevec is proving to be effective at controlling CML, but patients still have detectable disease at low levels [11]. Allogeneic bone-marrow or stem-cell transplantation (ABMT or ASCT) is the only known curative treatment for CML [13], and is thus the focus of this work.

There is an abundance of evidence that the immune system plays a critical role in the control of leukemia [1, 2, 9, 10, 12, 15], but the exact mechanism of action remains unclear. Infusion of allogeneic donor lymphocytes induces complete cytogenetic response (CR) in 75% of CML patients who relapse after ABMT [4, 7]. The enhanced efficacy of allogeneic over autologous SCT and the potent activity of donor lymphocyte infusion (DLI) have lead to the proposal of a graft-versus-leukemia (GVL) effect, which suggests that the donor lymphocytes mediate the removal of the cancer. Further evidence is found in the correlation between complete remission and both graft-versus-host disease (GVHD) and the loss of chimerism [8, 16]—but only when the donor hematopoietic cells prevail as the dominant lineage. Given that GVHD is mediated primarily by T cells, specifically CD8+ cells [6], the above evidence indicates a necessary role for donor T cells in cancer removal. Researchers have worked to dissect the mechanism by which donor T cells eliminate cancer, with varied results.

In this work, our goal is to simulate the immune dynamics of a stem-cell transplant in order to elucidate the mechanism of complete remission and to provide insight into potential future therapeutic strategies for treating CML. Our approach is based on following the time evolution of six cell populations: From the donor, we consider anti-cancer T cells (cells specific for leukemia and nothing else), anti-host T cells (those that would mediate a blood-restricted GVHD), and general donor blood cells. From the host, we consider cancer cells, anti-donor T cells (that may be responsible for graft rejection), and general host blood cells. The model is written in terms of a system of delayed differential equations (DDEs), using the delays to account for the progression of cells through various states.

We explore possible mechanisms behind a successful cure, whether mediated by a blood-restricted immune response or a cancer-specific graft-versus-leukemia (GVL) effect. Characteristic features of this model include sustained proliferation of T cells after initial stimulation, saturated T cell proliferation rate, and

the possible elimination of cancer cells, independent of fixed-point stability. In addition, we use numerical simulations to examine the effects of varying initial cell concentrations on the likelihood of a successful transplant. Among the observed trends, we note that higher initial concentrations of donor-derived, anti-host T cells slightly favor the chance of success, while higher initial concentrations of general host blood cells more significantly favor the chance of success. These observations lead to the hypothesis that anti-host T cells benefit from stimulation by general host blood cells, which induce them to proliferate to sufficient levels to eliminate cancer.

At present, DLI is a standard treatment for patients that relapse after a stem cell transplant, which for the purposes of our model provides an increase in T_H. While this does have a positive effect in eliminating the resurgent cancer, both within our model and biologically, our model suggests a novel treatment strategy: it may be more effective to infuse host cells, thus raising H and driving a stronger antigen response. These infusions would require prior irradiation or some other treatment to prevent the reintroduction of viable cancer cells, but would likely carry a lower risk of initiating GVHD, since the cells were originally taken from the host.

The timing of the infusion is also important in eliminating cancer. An open treatment question is whether preemptive DLI (before any evidence of a relapse) would be beneficial, reasoning that it may be better to go after the remaining cancer before waiting for a relapse. One problem with this approach is that there is no way to know a priori which patients will relapse and which are already cured, and hence some healthy patients will be subjected to the risks associated with an unnecessary procedure. We have already mentioned the potentially reduced risk of infusing host cells over donor cells, but in addition, the model indicates that a preemptive DLI using standard donor cells will be less effective than waiting for a relapse. This derives from the antigen driven response, where if the level of cancer is sufficiently low to be cytogenetically undetectable (as with patients in relapse), it will provide no supportive stimulus to the infused cells. Thus, the infusion will dwindle and die with only a small probability of locating and eliminating all of the few remaining cancer cells. In contrast, infusion of proxy cells that stimulate or maintain a blood-restricted GVHD response can keep the effector-cell-to-cancer ratio high for extended periods of time, maximizing the probability that the cancer will be eliminated.

The results of this work are summarized in [5].

REFERENCES

[1] E.P. Alyea, *et al.*, *Toxicity and efficacy of defined doses of CD4+ donor lymphocytes for treatment of relapse after allogeneic bone marrow transplant*, Blood **19** (1998), 3671–3680.
[2] A. Bagg, *Chronic myeloid leukemia: a minimalistic view of post-therapeutic monitoring*, Journal of Molecular Diagnostics **4** (2002), 1–10.
[3] F. Cervantes, *et al.*, *Long-term survivors in chronic granulocytic leukaemia: a study by the International CGL Prognosis Study Group*, Italian Cooperative CML Study Group. Br. J. Haematol. **87** (1994), 293–300.

[4] R.H. Collins, *et al.*, *Donor leukocyte infusions in 140 patients with relapsed malignancy after allogeneic bone marrow transplantation*, J. Clin. Oncol. **15** (1997), 433–444.

[5] R. DeConde, P. Kim, D. Levy, P.Lee, *Post transplantation dynamics of the immune response to chronic myelogenous leukemia*, J. Theor. Biology **236** (2005), 39–59.

[6] T. Klingebiel, P.G. Schlegel, *GVHD: overview on pathophysiology, incidence, clinical and biological features*, Bone Marrow Transplant **21** (1998), S45–S49.

[7] H.J. Kolb, *et al.*, *Graft-versus-leukemia effect of donor lymphocyte transfusions in marrow grafted patients. European Group for Blood and Marrow Transplantation Working Party Chronic Leukemia*, Blood **86** (1995), 2041–2050.

[8] K.-A. Kreuzer, *et al.*, *Kinetics of stem cell engraftment and clearance of leukaemia cells after allogeneic stem cell transplantation with reduced intensity conditioning in chronic myeloid leukaemia*, Eur. J. Haematol. **69** (2002), 7–10.

[9] W.A.E. Marijt, *et al.*, *Hematopoiesis-restricted minor histocompatibility antigens HA-1- or HA-2-specific T cells can induce complete remissions of relapsed leukemia*, Proc. Nat. Acad. Sciences **100** (2003), 2742–2747.

[10] J.J. Molldrem, *et al.*, *Evidence that specific T lymphocytes may participate in the elimination of chronic myelogenous leukemia*, Nature Medicine **6** (2000), 1018–1023.

[11] P. Paschka, *et al.*, *Molecular monitoring of response to imatinib (Glivec) in CML patients pretreated with interferon alphs. Low levels of residual disease are associated with continuous remission*, Leukemia **17** (2003), 1687–1694.

[12] C.L. Sawyers, *et al.*, *Imatinib induces hematologic and cytogenetic responses in patients with chronic myelogenous leukemia in myeloid blast crisis: results of a phase II study*, Blood **99** (2002), 3530–3539.

[13] C.A. Schiffer, R. Hehlmann, R. Larson, *Perspectives on the treatment of chronic phase and advanced phase CML and Philadelphia chromosome positive ALL*, Leukemia **17** (2003), 691–699.

[14] T. Tauchi, K. Ohyashiki, *Imatinib mesylate in combination with other chemotherapeutic agents for chronic myelogenous leukemia*, Int. J. Hematol. **79** (2004), 434–440.

[15] S.F.T. Thijsen, G.J. Schuurhuis, J.W. van Oostveen, G.J. Ossenkoppele, *Chronic mlyeloid leukemia from basics to bedside*, Leukemia **13** (1999), 1646–1674.

[16] M. Uzunel, *et al.*, *Kinetics of minimal residual disease and chimerism in patients with chronic myeloid leukemia after nonmyeloablative conditioning and allogeneic stem cell transplantation*, Blood **101** (2003), 469–472.

Modelling of moving boundaries with the phase-field method: Interfaces, membranes, and skins

MATHIS PLAPP

(joint work with Vincent Fleury, Thi-Hanh Nguyen)

Branched shapes are ubiquitous in nature. They are abundant in biological systems, both as parts of complex organisms (examples are organs such as lungs, kidneys, and the vascular tree) and as shapes taken by groups of organisms (coral trees, bacterial colonies). But they can also be created by purely abiotic processes such as crystallization (which can lead to symmetric shapes like snowflakes or irregular branched structures such as metal deposits on rocks), fingering of one liquid pushed into a region occupied by another, or crack formation. Whereas the mechanisms underlying the pattern formation processes in non-living systems are fairly well understood, the question to what extent the same processes also play

a role in biological pattern formation, and how the interplay of physical and biological processes creates the complex shapes of biological systems, is largely open [1].

From the point of view of mathematical modelling, a major challenge is to deal with the complicated shape of these objects, especially during growth when their geometry evolves with time. Classically, the equations of motion are formulated in terms of *moving boundary problems*, where the boundary can represent a surface, an interface between two distinct thermodynamic phases, a membrane, or a skin. The motion of this boundary is normally governed by fluxes of matter and/or energy which can arise inside and outside the growing structure. Furthermore, the physical properties on both sides of the boundary are often very different. Therefore, partial differential equations have to be solved separately inside and outside the structure and connected at the boundary in order to determine its motion. This requires an explicit representation of the boundary which is cumbersome for complex-shaped objects, especially in three dimensions.

An alternative approach to this kind of problems which has emerged in recent years is the *phase-field method*, in which an auxiliary field (phase field) is introduced, which is a smoothed indicator function; the boundary in then represented by a level set of this function. In contrast to the so-called *level set method*, in which a signed distance function is used instead of a smoothed indicator function, the phase field often has a direct physical interpretation as an order parameter or density. The advantage is that an equation of motion can then be obtained from basic principles of out-of-equilibrium thermodynamics. Most commonly, this equation is a Ginzburg-Landau type equation which can be obtained from a free energy functional and which is coupled to the other variables of the problem. All physical properties are then interpolated trough a diffuse but thin interface. The new coupled problem can be solved without explicit knowledge where the boundary is, which leads to great simplification of the numerics. The connection between the phase-field model and the classic moving boundary problem is established by matched asymptotic expansions.

In its beginnings, the phase-field method was developed mainly to describe phase transformations in materials, such as precipitation [2] or solidification (for a recent review, see [3]). More recently, the method has been extended to number of different moving boundary problems, including fracture [4], polyphase flows [5], and electrocrystallization [6]. Furthermore, applications to biological systems start to emerge, for example the modelling of vesicle motion in shear flows [7].

We have developed a phase-field model for the equilibrium and growth shapes of fiber-covered surfaces. This is originally motivated by the observation that many organs of complex organisms are branched, but different organs can exhibit very different architectures, ranging from ordered, dichotomous branching to quite random structures. It is known from crystal growth that the detailed structure of the interface, and above all its anisotropy, play a crucial role in shaping ramified structures. For instance, the regular shape of a snowflake is created by the underlying crystal structure. In biological systems, there is no crystalline structure; however,

the "skins" of many organs exhibit line patterns created by arrangements of fibroblasts and/or collagen fibers. This creates an anisotropic bending rigidity: the surface is easier to bend in the direction normal to the fibers than in the direction parallel to the fibers. We have developed a phase-field model that can determine the optimal form of line patterns on arbitrary surfaces and explore the effects of this anisotropy. The main ingredients of the model are the following.

- The geometry of the surface is described by a scalar phase field ϕ.
- Growth is limited by diffusion of a scalar quantity u, in analogy with crystal growth and viscous fingering. This mode of growth is the simplest one which leads to the self-organized emergence of ramified structures.
- The fiber pattern is described by a traceless tensor Q_{ij} of rank two, in analogy with nematic liquid crystals. This is motivated by the fact that, for example, fibroblasts or other cells exhibit local orientational order and the same topological defects as nematic liquid crystals [8].
- The fiber pattern is localized at the surface by including a suitable coupling to the phase field. The fibers are forced to remain tangential to the surface by an anchoring term.
- The anisotropic bending rigidity is implemented by a contraction of the curvature tensor with the tensorial order parameter Q_{ij}.

Preliminary simulations using this model yield the following results:

- The model is able to find optimal line patterns for any given geometry of the surface.
- The anisotropic bending rigidity creates equilibrium shapes in which high curvatures occur in directions normal to the predominant fiber direction.
- Topological singularities are attracted to regions of the surface with high curvature.
- As a result, the singularities move to the tips of branches created by the instability of an initial round shape, and trigger a fast growth of slender branches with sharp tips ("thorns").

Such growth patterns cannot be observed with a "classical" anisotropy such as found in crystals. Our results therefore demonstrate that the presence of fibers together with an anisotropic bending rigidity can create new and unique growth shapes. The relevance of this mechanism to biological pattern formation, however, has yet to be assessed.

References

[1] *Branching in nature*, edited by V. Fleury, J.-F. Gouyet and M. Leonetti, Springer/EDP Sciences (2001).
[2] A.G. Khatchaturyon, *Theory of Structural Transformations in Solids*, Wiley, New York (1983).
[3] W.J. Boettinger, J.A. Warren, C. Beckermann and A. Karma, Annu. Rev. Mater. Res. **32** (2002), 163.
[4] A. Karma, D.A. Kessler and H. Levine, Phys. Rev. Lett. **87** (2001), 045501.
[5] D. Jacqmin, J. Comp. Phys. **155** (1999), 1.

[6] J.E. Guyer, W.J. Boettinger, J.A. Warren and G.B. McFadden, Phys. Rev. E **69** (2004), 021603.
[7] T. Biben and C. Misbah, Phys. Rev. E **67** (2003), 031908.
[8] R. Kemkemer, D. Kling, D. Kaufmann and H. Gruler, Eur. Phys. J. E **1** (2000), 215.

New dimension in Biology: two examples of 3D phenomenological models

Giovanni Naldi

Although computational and experimental models for cell migration and dynamics on two-dimensional (2D) substrata have described how various molecular and cellular properties and biochemical processes are integrated to accomplish cell functions, biologists are increasingly turning to three-dimensional cell cultures, where they are discovering biological activities that more closely mirror what happens in living organisms (see e.g [1, 10, 9]). In fact, the in situ environment of a cell in living organism has a three-dimensional architecture. This "new dimension" may represent a challenge in mathematical and computational modelling in order to better understand physiological and biochemical processes. We report here two examples regarding phenomenological description of early stages of vascular network assembly [4] and, respectively, of olfactory system in embryogenesis [2].

Mathematical models in 3D Vasculogenesis. Vascular networks [3] form by the spontaneous aggregation of individual endothelial cells migrating toward vascularization sites (vasculogenesis). The study of this process is performed by biologists using in vitro and in vivo assays, both in two-dimensional and, recently, three-dimensional settings. A succesfull theoretical model of two-dimensional experimental vasculogenesis has been recently proposed [5, 8], showing the relevance of percolation concepts and of cell cross-talk (chemotactic autocrine loop) to the understanding of the self-aggregation process. We study the natural 3D extension of the earlier proposed computational model, which we take as a starting point for the investigation of the genuinely three-dimensional process of vasculogenesis in vertebrate embryos. The computational and phenomenological model obtained by experimental data is based on the following system for the cell density $n(x,t)$, their velocity field $\mathbf{v}$ and for the concentration field $c(x,t)$ of the soluble chemical factors ($\mathbf{x} \in \mathbf{R}^d$, $d = 2, 3$ is the space variable, and $t \geq 0$ is the time variable),

$$(1) \quad \begin{cases} \frac{\partial n}{\partial t} + \nabla \cdot (n\mathbf{v}) = 0 \\[2mm] \frac{\partial \mathbf{v}}{\partial t} + \mathbf{v} \cdot \nabla \mathbf{v} = \mu(c)\nabla c - \nabla \phi(n) - \beta(c)\mathbf{v} \\[2mm] \frac{\partial c}{\partial t} = D\Delta c + \alpha(c)n - \frac{c}{\tau} \end{cases}$$

Here μ measures the cell response to the chemotactic factor, while D and τ are respectively the diffusion coefficient and the characteristic degradation time of the soluble chemoattractant. Finally the function α determines the rate of release of the chemical factor. The friction term $-\beta\mathbf{v}$ mimics the adhesion of the cells to the
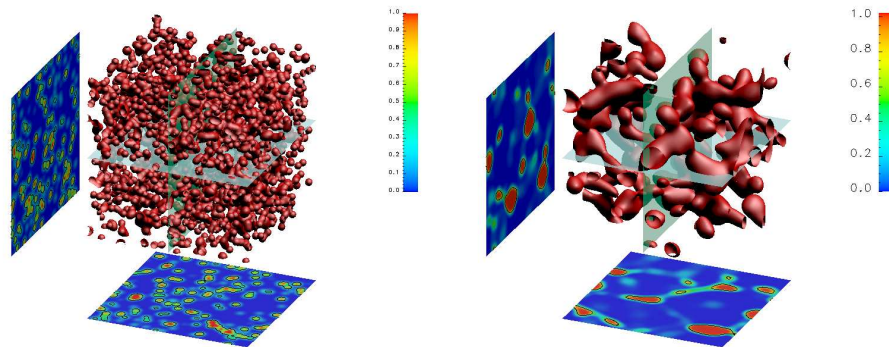
FIGURE 1. Plot of the initial and stationary state of a numerical simulation with 2500 cells/mm^3. A well developed network-like structures is observed

extracellular matrix while the term $\nabla\phi(n)$ is a density dependent pressure term where $\phi(n)$ is zero for low densities, and increases for densities above a suitable threshold: this pressure is a phenomenological term which models short range interaction between cells. The numerical approximation of the model poses several technical problems. Starting from initial conditions mimicking the experimentally observed ones the numerical simulations produce network-like structures qualitatively similar to those observed in the early stages of in vivo vasculogenesis. Our numerical scheme is obtained by a suitable relaxed approximation [6, 7] and by coupling IMEX schemes for time integration and ENO-WENO schemes for space discretization. A numerical simulation with randomly assigned initial cell positions is shown in Figure 1. Theoretical and numerical analysis of the proposed models are under study. We are also developing the computation of critical percolative indices as a robust measure of the network geometry. This is a joint work with F. Cavalli and M. Semplice (University of Milano), A. Gamba and G. Puppo (Politecnico di Torino, Italy), and G. Serini (Institute for Cancer Research and Treatment, Italy).

Olfactory system in embryogenesis. The olfactory system is formed by the coordinated development of two embryonic structures: the olfactory placode (OPL) and the anterior forebrain (FB), precursors of the olfactory epithelium (OE) and olfactory bulb (OB), respectively. Olfactory axons elongate from the OPL and reach FB where they establish the primitive connections. The molecular signals that control early patterning and axon extension are beginning to be functionally characterized. However, little is known about axon-mesoderm and forebrain-mesoderm signals. A 3D reconstruction and an associated mathematical model of the olfactory development is being generated, that might help to decipher the relationships between all the variables involved. The first results indicate the existence of a complex interplay between cells of different embryonic origins for the establishment of olfactory connections, in which Wnt signals play a key role. Numerical simulations of the olfactory placode are performed by using simple discrete scheme

with stochastic terms in order to reproduce the biological environment. A complete model involving genetic information is under study. Biological experiments, data and support come from G. Merlo, A. Zaghetto, and M. Gozzo (Dulbecco Telethon Institute, Italy). The modelling and numerical simulations are joint work with G. Aletti and P. Causin (Universityt of Milano).

References

[1] A. Abbott, *Cell culture: biology's new dimension*, Nature **424** (2003), 870–2.
[2] G. Aletti, P. Causin, M. Gozzo, G. Merlo, G. Naldi and A. Zaghetto, *Computational Model for olfactory system formation in embryogenesis*. In preparation.
[3] P. Carmeliet, *Mechanisms of angiogenesis and arteriogenesis*, Nature Medicine **6** (2000), 389–395.
[4] F. Cavalli, A. Gamba, G. Naldi, M. Semplice and G. Serini, *Percolative analysis of 3D vasculogenesis*, Submitted to Proceedings CMSB 2006.
[5] A. Gamba, D. Ambrosi, A. Coniglio, A. de Candia, S. Di Talia, E. Giraudo, G. Serini, L. Preziosi and F. Bussolino, *Percolation, morphogenesis, and Burgers dynamics in blood vessels formation*, Phys. Rev. Lett. **90** (2003), 118101.
[6] S. Jin and Z. Xin, *The relaxation schemes for systems of conservation laws in arbitrary space dimension*, Comm. Pure and Appl. Math. **48** (1995), 235–276.
[7] G. Naldi and L. Pareschi, *Numerical schemes for hyperbolic systems of conservation laws with stiff diffusive relaxation*, SIAM J. Numer. Anal. **37** (2000), 1246–1270.
[8] G. Serini, D. Ambrosi, E. Giraudo, A. Gamba, L. Preziosi and F. Bussolino, *Modeling the early stages of vascular network assembly*, EMBO J. **22** (2003), 1771–9.
[9] L.E. O'Brien, M.M.P. Zegers, and K.E. Mostov, *Building epithelial architecture: insights from three-dimensional culture models*, Nature Reviews, Molecula Cell Biology **3** (2002), 531–537.
[10] S. Zhang, *Beyond the Petri dish*, Nature Biotechnology **22** (2004), 151–2.

Gradient-driven dynamic pattern formation in mathematical models of cancer cell invasion of tissue

Mark A.J. Chaplain

The growth of solid tumours proceeds through two distinct phases: the avascular and the vascular phase. It is during the latter stage that the insidious process of cancer invasion of peritumoral tissue can and does take place. Vascular tumours grow rapidly allowing the cancer cells to establish a new colony in distant organs, a process that is known as metastasis. The progression from a single, primary tumour to multiple tumours in distant sites throughout the body is known as the metastatic cascade. This is a multistep process that first involves the overexpression by the cancer cells of proteolytic enzyme activity, such as the urokinase-type plasminogen activator (uPA) and matrix metalloproteinases (MMPs). uPA itself initiates the activation of an enzymatic cascade that primarily involves the activation of plasminogen and subsequently its matrix degrading protein plasmin. Degradation of the matrix then enables the cancer cells to migrate through the tisse and subsequently to spread to secondary sites in the body.

In this talk we consider a mathematical model of cancer cell invasion of tissue (extracellular matrix) which focuses on the role of the the plasminogen activation system. The model consists of a system of reaction-diffusion-taxis partial differential equations describing the interactions between cancer cells, urokinase plasminogen activator (uPA), uPA inhibitors, plasmin and the host tissue. The focus of the modelling is on the spatio-temporal dynamics of the uPA system and how this influences the migratory properties of the cancer cells through random motility, chemotaxis and haptotaxis. The results obtained from numerical computations carried out on the model equations produce rich, dynamic heterogeneous spatio-temporal solutions and demonstrate the ability of rather simple models to produce complicated dynamics, all of which are associated with tumour heterogeneity and cancer cell progression and invasion. Full details of the model can be found in the paper of Chaplain and Lolas (2005).

The specific system to be studied is the following:

$$\frac{\partial c}{\partial t} = \underbrace{D_c \frac{\partial^2 c}{\partial x^2}}_{\text{Random Motion}} - \frac{\partial}{\partial x} (\underbrace{\chi_c c \frac{\partial u}{\partial x}}_{\text{uPA-chemo}} + \underbrace{\zeta_c c \frac{\partial p}{\partial x}}_{\text{PAI-1-chemo}} + \underbrace{\xi_c c \frac{\partial v}{\partial x}}_{\text{VN-hapto}}) + \underbrace{\mu_1 c (1-c)}_{\text{proliferation}},$$

$$\frac{\partial v}{\partial t} = \underbrace{-\delta v m}_{\text{degradation}} + \underbrace{\phi_{21} u p}_{\text{uPA/PAI-1}} - \underbrace{\phi_{22} v p}_{\text{PAI-1/VN}} + \underbrace{\mu_2 v (1-v)}_{\text{proliferation}},$$

$$\frac{\partial u}{\partial t} = \underbrace{D_u \frac{\partial^2 u}{\partial x^2}}_{\text{Diffusion}} - \underbrace{\phi_{31} p u}_{\text{PAI-1/uPA}} - \underbrace{\phi_{33} c u}_{\text{uPA/cells}} + \underbrace{\alpha_{31} c}_{\text{production}} ,$$

$$\frac{\partial p}{\partial t} = \underbrace{D_p \frac{\partial^2 p}{\partial x^2}}_{\text{Diffusion}} - \underbrace{\phi_{41} p u}_{\text{PAI-1/uPA}} - \underbrace{\phi_{42} p v}_{\text{PAI-1/VN}} + \underbrace{\alpha_{41} m}_{\text{production}} ,$$

$$\frac{\partial m}{\partial t} = \underbrace{D_m \frac{\partial^2 m}{\partial x^2}}_{\text{Diffusion}} - \underbrace{\phi_{51} p u}_{\text{PAI-1/uPA}} + \underbrace{\phi_{52} p v}_{\text{PAI-1/VN}} + \underbrace{\phi_{53} u c}_{\text{uPA/cells}} .$$

This is solved numerically in 1D and 2D domains with appropriate initial data and boundary conditions.

References

[1] A.R.A. Anderson, *A hybrid mathematical model of solid tumour invasion: The importance of cell adhesion*, Math. Med. Biol. **22** (2005), 163–186.

[2] A.R.A. Anderson, M.A.J. Chaplain, E.L. Newman, R.J.C. Steele and A.M. Thompson, *Mathematical modelling of tumour invasion and metastasis*, Journal of Theoretical Medicine **2** (2000), 129–154.

[3] N. Bellomo, A. Bellouquid and E. De Angelis, *The modelling of the immune competition by generalized kinetic (Boltzmann) models: Review and research perspectives*, Mathematical and Computer Modelling **37** (2003), 1131–1142.

[4] H.M. Byrne, M.A.J. Chaplain, G.J. Pettet and D.L.S. McElwain, *A mathematical model of trophoblast invasion*, Journal of Theoretical Medicine **1** (1998), 275–286.

[5] H.M. Byrne, M.A.J. Chaplain, G.J. Pettet and D.L.S. McElwain, *An analysis of a mathematical model of trophoblast invasion*, Applied Mathematics Letters **14** (2001), 1005–1010.

[6] M.A.J. Chaplain, *The mathematical modelling of tumour angiogenesis and invasion*, Acta Biotheoretica **43** (1995), 387–402.

[7] M.A.J. Chaplain and G. Lolas, *Mathematical modelling of cancer cell invasion of tissue: The role of the urokinase plasminogen activation system*, Mathematical Models and Methods in Applied Sciences **15** (2005), 1685–1734.

[8] R.A. Gatenby, *Models of tumour-host interaction as competing populations: Implications for tumor biology and treatment*, Journal of Theoretical Biology **176** (1995), 447–455.

[9] R.A. Gatenby and E.T. Gawlinski, *A reaction-diffusion model of cancer invasion*, Cancer Research **56** (1996), 5745–5753.

[10] M. Lachowicz, *Micro and meso scales of description corresponding to a model of tissue invasion by solid tumours*, Mathematical Models and Methods in Applied Sciences **15** (2005), 1667–1683.

[11] M.E. Orme and M.A.J. Chaplain, *A mathematical model of vascular tumour growth and invasion*, Mathematical and Computer Modelling **23** (1996), 43–60.

[12] M.E. Orme and M.A.J. Chaplain, *Two-dimensional models of tumour angiogenesis and anti-angiogenesis strategies*, IMA Journal of Mathematics Applied in Medicine & Biology **14** (1997), 189–205.

[13] A.J. Perumpanani, J.A. Sherratt, J. Norbury, H.M. Byrne, *Biological inferences from a mathematical model for malignant invasion*, Invasion & Metastasis **16** (1996), 209–221.

[14] A.J. Perumpanani, D.L. Simmons, A.J.H. Gearing, K.M. Miller, G. Ward, J. Norbury, M. Schneemann and J.A. Sherratt, *Extracellular matrix-mediated chemotaxis can impede cell migration*, Proceedings of the Royal Society of London, Series B **265** (1998), 2347–2352.

[15] A.J. Perumpanani and H.M. Byrne, *Extracellular matrix concentration exerts selection pressure on invasive cells*, European Journal of Cancer **35** (1999), 1274–1280.

[16] L. Preziosi (Ed.), *Cancer Modelling and Simulation*, Chapman & Hall/CRC Press (2003).

The encapsulation of particles and bubbles by an advancing solidification front in cryopreservation

Stephen H. Davis

(joint work with Min S. Park, Alexander A. Golovin)

Cryopreservation is used to store and transport biological tissue. Among the scientific issues involved are the stresses to which the cell is exposed and the possibility that upon remelting the cell will be functional.

To begin such a study, we examine the fate of solid spheres and spherical bubbles approached by a solidification front. Such an insoluble particle, submerged in a liquid and approached by an advancing solidification front, may be captured by the front or rejected. The particle behavior is determined by an interplay among van der Waals interactions, thermal conductivity differences between the particle and melt, solid-liquid interfacial energy, the density change caused by the liquid-solid phase transition, and in the case of a bubble, the Marangoni effect at the liquid-gas interface. We calculate the particle velocity and the deformation of the front when the particle is close to the front, using the lubrication approximation, and

investigate how the particle speed, relative to the front, depends on the parameters that characterize the described effects.

Rather than detailing the analysis, we give the results in which in the simplest case involves repulsion due to van der Waals forces and attractions due to hydrodynamic forces. How these two balance determines the velocity u of the particle sensed away from the front, which moves at velocity V in the same direction. Figure 1a shows u versus δ_0, the minimum gap between particle and front. When $V > u_{\max}$, the front overtakes the particle and captures it. When $V < u_{\max}$ there are two possibilities: (i) $\delta_0 > \delta_u$ and there is evolution to the point $u = V$ at $\delta_0 = \delta_s$, after which the spacing remains constant, and (ii) if δ_0 is small enough, $\delta_0 < \delta_u$, then encapsulation takes place. The remaining figures illustrate how the additional physical effects act. Of course the next step is to model a cell with a semi-permeable, elastic membrane surrounding a gel-like interior.

<div align="center">References</div>

[1] M.S. Park, A.A. Golovin and S.H. Davis, Journal of Fluid Mechanics (2006), in press.

<div align="center">

Diffusion and Homogenization in Phototransduction

Daniele Andreucci, Giovanni Caruso, Heidi Hamm

</div>

The talk was divided into three parts, delivered by Heidi Hamm, Daniele Andreucci and Giovanni Caruso, introducing respectively the biological, mathematical and numerical aspects of the problem.

<div align="center">

1. Diffusion in the rod outer segment

</div>

The phototransduction cascade is a quite complex sequence of chemical reactions and diffusion phenomena taking place in the retina photoreceptors. We deal here with the rod, and more specifically with the processes taking place in the rod outer segment (ROS); we refer to [1] for more information.

With reference to Figure 1, we recall that the space available for diffusion of the species cGMP and Ca is the part outside of the discs (which are represented as black boxes). The output of the model we are mainly interested in, i.e., the current (see Section 2), is linked to the flux of $[\mathrm{Ca}^{2+}]$ across the outer boundary; however we focus here on the diffusion-reaction problem for [cGMP], for the sake of brevity.

We simplify the complex geometry of the rod outer segment (ROS) by means of the mathematical devices of concentration of capacity and homogenization (see also Figure 1 for notation).

Namely, the *outer shell*

$$\Sigma_\varepsilon = \{R < |\,\bar{x}\,| < R + \sigma\varepsilon\,, 0 < z < H\}\,,$$

the incisure

$$\mathcal{B}_\varepsilon = \{\bar{x} \in \mathcal{V}_\varepsilon\,, 0 < z < H\}\,,$$
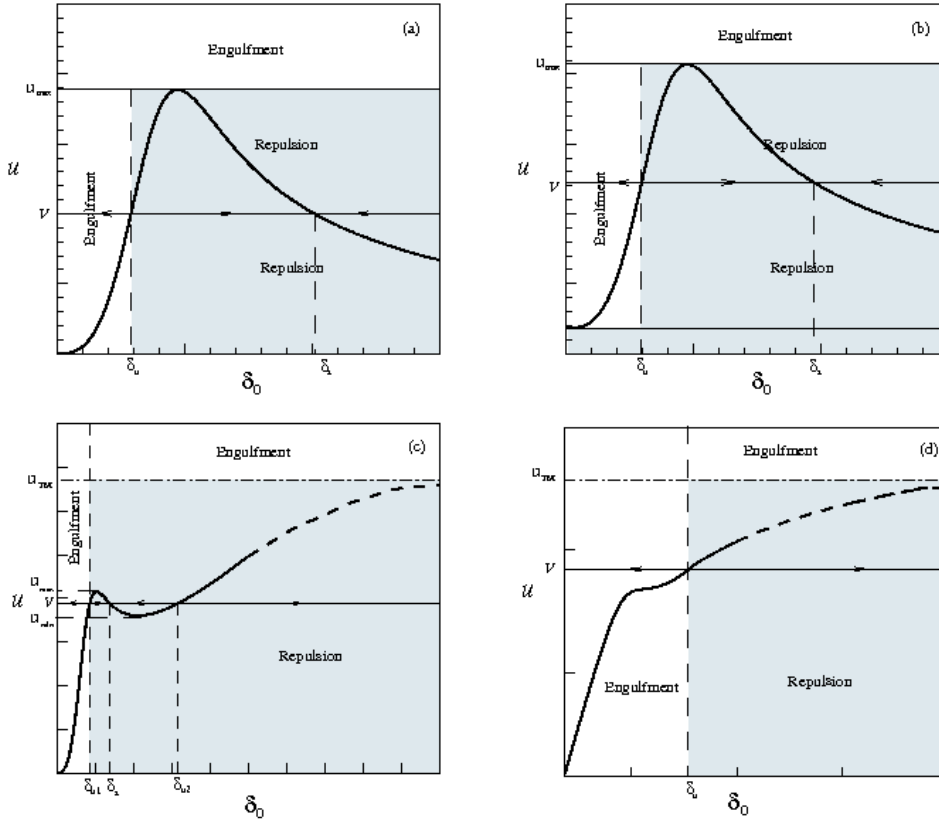
FIGURE 1. Schematic representation of engulfment conditions based on the dependence of a particle or bubble dimensionless speed on the dimensionless separation distance from the front, $u(\delta_0)$. (a) typical dependence $u(\delta_0)$ with one maximum; δ_u - unstable steady state, δ_e - stable steady state, (b) dependence $u(\delta_0)$ for a solid particle in the presence of the bulk flow caused by the density change upon solidification; (c) dependence $u(\delta_0)$ for a bubble with thermocapillary effect with two extrema; dashed line corresponds to an asymptotic value of thermocapillary migration speed which is beyond the validity of the lubrication approximation; (d) monotonic dependence $u(\delta_0)$ for a bubble with thermocapillary effect for large Marangoni numbers.

and the interdiscal space I_j^* adjacent to the activation site are concentrated, while the rest of the interior cylinder

$$\Omega = \{ \mid \bar{x} \mid < R, 0 < z < H \}$$
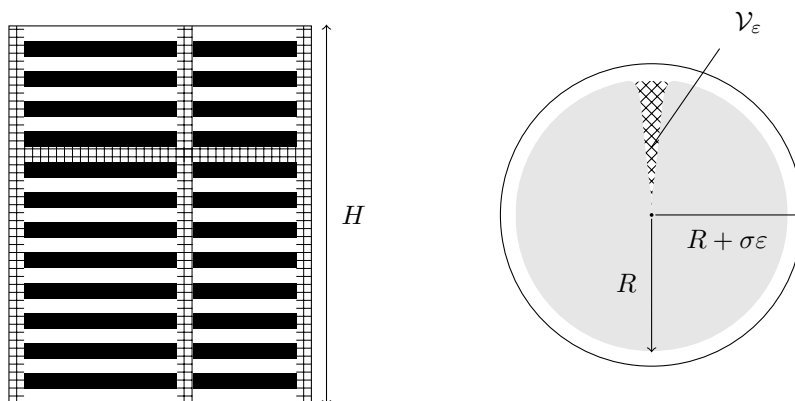
FIGURE 1. *Left* side view. The shaded area is the region undergoing con-
centration of capacity as $\varepsilon \to 0$. *Right*: top view. The widths ε of the discs,
$\sigma\varepsilon$ of the outer shell, $\nu\varepsilon$ of the interdiscal spaces, as well as the maximum
width of the incisure $\mathcal{V}_\varepsilon$, are much smaller than R and H. Typical dimensions
(for the salamander) are: $H \simeq 20\text{–}28\,\mu\text{m}$, $R \simeq 5.5\,\mu\text{m}$, $\varepsilon \simeq 0.01\text{–}0.014\,\mu\text{m}$,
$\sigma \simeq 1$, $\nu \simeq 1$. The total number of discs ranges in 800–1000. The axial
coordinate is denoted by z, and the transversal coordinates by $\bar{x} = (x_1, x_2)$.

is homogenized as $\varepsilon \to 0$. Technically we achieve this result in the limit $\varepsilon \to 0$ by
introducing the sequence of approximating equations for diffusion in the cytosol

$$(1) \qquad a_\varepsilon(x)\frac{\partial u_\varepsilon}{\partial t} - \nabla \cdot \big(D_{\text{cG}}a_\varepsilon(x)\nabla u_\varepsilon\big) = 0\,,$$

where we have set $u_\varepsilon = [\text{cGMP}]$, and

$$a_\varepsilon(x) = \begin{cases} \dfrac{\varepsilon_o}{\varepsilon}\,, & \text{in the regions to be concentrated: } \Sigma_\varepsilon,\ \mathcal{B}_\varepsilon,\ I_j^*; \\[2mm] 1\,, & \text{elsewhere in the cytosol.} \end{cases}$$

Here ε_o denotes the physical value of ε. The variable $v_\varepsilon = [\text{Ca}^{2+}]$ satisfies a similar
equation.

The problem is completed by suitable initial and boundary data. For example,
the boundary flux condition for u_ε on the side of the discs is

$$(2) \qquad \nabla u_\varepsilon \cdot \overrightarrow{n}_{\text{out}} = -\frac{1}{2}\nu\varepsilon\big(\beta u_\varepsilon - \alpha(v_\varepsilon)\big) - \chi_{\{z=z_*\}}[\text{PDE}^*]_\sigma u_\varepsilon\,,$$

where z_* is the level corresponding to the activated side. The first term on the right
hand side of (2) corresponds to the chemical activity on *all* discs and therefore
contains the homogenization scaling factor ε, while the second term accounts for
depletion of cGMP by activated PDE and appears only on the side hit by the
photon.

In the limit we obtain a set of diffusion equations in the domains Ω, and

$$\Sigma = \lim \Sigma_\varepsilon = \{|\ \bar{x}\ | = R\,, 0 < z < H\}\,,$$
$$\mathcal{B} = \lim \mathcal{B}_\varepsilon = \{r_o < x_1 < R\,, x_2 = 0\,, 0 < z < H\}\,,$$
$$D_R = \lim I_j^* = \{|\ \bar{x}\ | < R\}\,.$$

Note that Σ, $\mathcal{B}$, and D_R are surfaces so that the diffusion operator on them must be understood in the suitable sense. The equations are coupled in two ways: first, the limits of u_ε in the different compartments agree on the intersections of their domains; second, the mass exchanges between compartments appear as sources in the relevant diffusion equations. We refer for more details to [1], [2], [3].

2. Numerical setup

A finite element scheme is here presented and used to obtain a numerical solution of the nonlinear diffusion equations relevant to the phototransduction homogenized model described in section 1. To this end a weak form of the governing equations is considered [2], not reported here for the sake of brevity, suitable for the application of the finite-element method.

The equations are set in a domain composed of a cylinder (the interior of the rod), its lateral boundary (the outer shell), several rectangular surfaces cutting the cylinder along radial directions (the incisures) and some circular cross sections (the activated discs). Due to the homogenization technique used in the analysis, the intricate geometry of the rod, containing 800 discs, has disappeared and the homogenized equations are set in homogeneous domains, which can be efficiently discretized by a relatively small number of elements. This implies a relevant reduction in the time required to perform the numerical computations; moreover, as shown in [4], the obtained results are in close agreement with the ones obtained using a model of the rod taking into account its actual intricate geometry.

A dedicated program in Matlab language has been developed, capable of incorporating any number of incisures and any number of activation sites, with any given distribution on the ROS. Thus the code is aimed at being an operational tool to perform numerical experiments of phototransduction, in rods of different geometry and structure, under a wide spectrum of operating conditions. A finite element mesh is created by using six-node prismatic elements for the interior of the rod, four-node rectangular elements for the outer shell and the blades relevant to each incisure, and three-node triangular elements for each of the activated discs. As the greatest rates of change occur near the activated disc, a mesh-generation algorithm has been written to accomplish local logarithmic refinements of the mesh in a chosen region around each of the activated discs. This enables us to obtain an accurate solution using fewer elements, thereby considerably reducing the computational cost. In Figures 2 and 3 a typical mesh of a salamander rod outer segment is reported; the rod contains 23 incisures and a photon activates the disc placed at half height of the rod.

Time integration was performed with the Crank-Nicolson scheme, which guarantees stability and convergence without requiring too small time steps. The
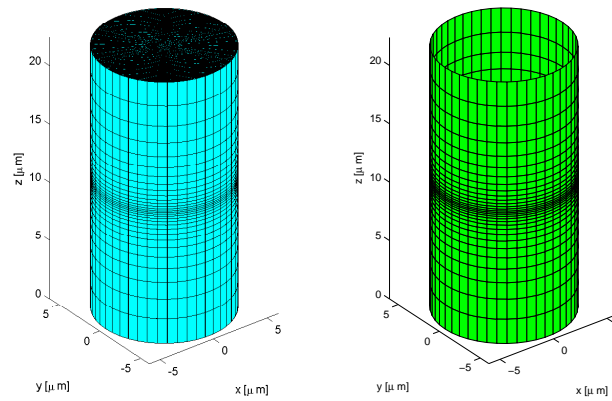
FIGURE 2. Mesh of the interior (*left*) and outer shell (*right*).
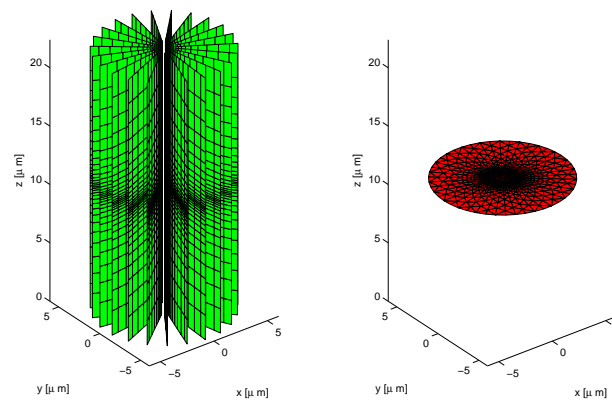
FIGURE 3. Mesh of the incisures (*left*) and of the activated disc (*right*).

nonlinear forcing terms have been approximated, within each element, by interpolating their nodal values. Their nodal values have been computed at the current time-step by weighting the values at the old and new time, as prescribed by the semi-implicit integration method. Accordingly, an iterative procedure has been used to advance the solution to the new time.

Simulation results. The numerical solution computed by the matlab program is expressed in terms of the nodal concentrations [cGMP] and [Ca^{2+}] at each considered time. Then the local current density $J(\theta; z; t)$ can be evaluated in terms of the nodal values of [cGMP] and [Ca^{2+}] on the outer shell. The global
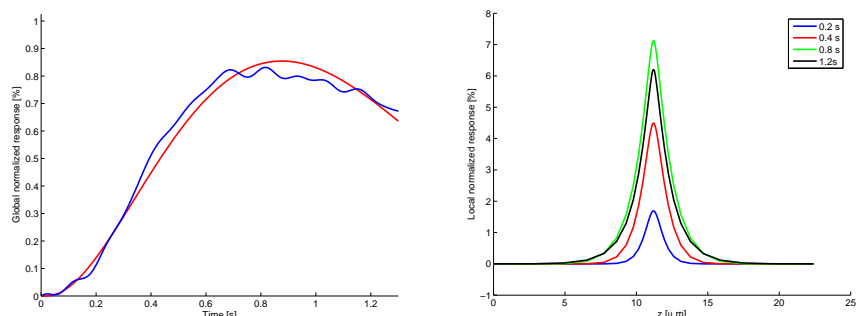
FIGURE 4. Global normalized response (left) and local normal-
ized response at different times (right).

current $i(t)$ across the entire plasma membrane is the surface integral of the cur-
rent density over the lateral boundary of the ROS. Results can be presented in
terms of the global relative response $i(t)_{\mathrm{dark}} - i(t)$, the global normalized response
$1 - i(t)/i(t)_{\mathrm{dark}}$, and local normalized response $1 - J(\theta; z; t)/J_{\mathrm{dark}}$, where 'dark'
denotes quantities in the dark. As an example, at the left of Figure 4 the global
normalized response is reported for a simulation of the typical salamander single
photon response; peak time occurs at about 0.8s and the maximum normalized
drop of global current is about 0.8%. The superimposed (less smooth) curve
has been obtained by averaging several experimental single photon responses on
salamander rods (F. Rieke). On the right part of Figure 4 the local normalized
response along a vertical line of the outer shell is reported for different times; it
clearly appears that just a small portion of the outer shell around the activated
disc contributes to the visual signal, thus confirming the localized nature of the
single photon response.

These are just some of the possible outputs produced by the Matlab program;
concentrations [cGMP] and [Ca^{2+}] can be computed at any location in the rod
and visualizations of the current density evolving in the time at any position of
the outer shell are possible. Many kinds of analysis can be performed, by varying
the geometry of the rod, the number and positions of incisures and the number
and positions of the photons hitting the proteinic discs. To this end, a detailed
study about the influence of incisures on the phototransduction signal is presented
in [5]. Moreover it is possible to consider different typologies of activation models
and take into account several effects as random walk of rhodopsin, deterministic
or stochastic sudden shutoff of rhodopsin or different phosphorylation states for
rhodopsin.

REFERENCES

[1] D. Andreucci, P. Bisegna, G. Caruso, H.E. Hamm and E. DiBenedetto, *Mathematical model
of the spatio-temporal dynamics of second messangers in visual transduction*, Biophysical
Journal **85** (2003), 1358–1376.

[2] D. Andreucci, P. Bisegna and E. DiBenedetto, *Homogenization and Concentrated Capacity for The Heat Equation with Non–Linear Variational Data In Reticular Almost Disconnected Structures and Applications to Visual Transduction*, Annali di Matematica Pura e Applicata **182** (2003), 375–407.

[3] D. Andreucci, P. Bisegna and E. DiBenedetto, *Homogenization and Concentration of Capacity in the Rod Outer Segment with Incisures*, Applicable Analysis **85** (2006), 303–331.

[4] G. Caruso, H. Khanal, V. Alexiades, F. Rieke, H.E. Hamm and E. DiBenedetto, *Mathematical and computational modelling of spatio-temporal signalling in rod phototransduction*, System Biology **152** (2005), 119–137.

[5] G. Caruso, P. Bisegna, L. Shen, D. Andreucci, H.E. Hamm and E. DiBenedetto, *Modeling the Role of Incisures in Vertebrate Phototransduction*, Biophysical Journal, to appear.

Population-scale modelling of cellular chemotaxis and aggregation

J.R. KING

(joint work with J.A. Fozard)

1. FORMULATION

We seek here to examine the effects of aggregation on the movement of populations of cells. The approach we adopt goes to the opposite extreme from most (e.g. Keller-Segel-based) models for chemotactically-driven aggregation, which neglect entirely the effects on their motility of cells binding to one another, by studying a paradigm problem in which only single cells are motile. Thus the model we use is an extension of the Becker-Döring aggregation equations in which single cells undergo diffusion as well as attaching themselves to clusters of any size, and we examine in particular the large-time behaviour of the solutions to two specific initial boundary problems, which have relevance to aggregation in chemotaxis assays.

We consider a population of identical cells undergoing both random motion and chemotaxis (directed motion under the influence of a chemical stimulus) and sticking together following collisions. Clusters of more than one cell are considered to be immobile, and so grow further only through additional single cells colliding with them. We ignore the effects of cell division and the chemoattractant is here taken to be introduced exogenously (i.e. the only mechanism driving aggregation is cell-cell adhesion). The aggregation process varies in one dimension, with single cells undergoing net advection and diffusion in that direction. In allowing the problem to be inhomogeneous in this particular dimension, we view all quantities as averages over the perpendicular cross section.

Combining the Becker-Döring equations [1] (without fragmentation) with the usual transport terms (cf. the Keller-Segel model [2]), we obtain

$$(1) \quad \frac{\partial c_1}{\partial t} + \frac{\partial}{\partial x}\left(\chi \frac{\partial f}{\partial x} c_1\right) = \frac{\partial}{\partial x}\left(D \frac{\partial c_1}{\partial x}\right) - a_1 c_1^2 - \sum_{j=1}^{\infty} a_j c_1 c_j,$$

$$(2) \qquad \frac{\partial c_n}{\partial t} = a_{n-1} c_1 c_{n-1} - a_n c_1 c_n, \qquad\qquad n \geq 2,$$

where $c_n(x,t)$ is the concentration of clusters of size n. The parameters here are the rate coefficients a_n, the random motility coefficient D and the chemotactic coefficient χ, all of which are taken to be constant; f is the prescribed distribution of a chemotactic signal, which (in the interests of treating the simplest possible problem of the current class) we take to be at the linear steady state $f(x) = f_0 + f_1 x$. We examine the above equations with rate coefficients of power-law form

$$(3) \qquad a_n = \alpha n^p, \qquad \text{with } \alpha > 0, \quad 0 \le p \le 1,$$

as this allows us to encompass a variety of cases of interest; the choice $p = 1/3$ is appropriate when the clusters are compact and spherical for large n.

The first problem we address is the Cauchy Problem on the whole real line, with a localised initial distribution of cells, $c_1 = F(x)$. This is in principle of relevance to "sandwich" assays for chemotaxis [3], in which a thin layer of cells is placed between two layers of collagen gel, and differing concentrations of chemotactic factors are introduced into the upper and lower layers. In the second situation (the Cauchy-Dirichlet Problem) we instead impose the boundary condition

$$(4) \qquad c_1 = C \quad \text{at } x = 0$$

for some positive constant C, and examine the behaviour of the solution in the semi-infinite domain $x > 0$. This is representative of the behaviour in an "under-agarose" assay for chemotaxis [4], the boundary condition (4) corresponding to a well containing a given concentration of cells. The problem can be written in dimensionless form (containing only two parameters, U and p) as

$$(5) \quad \frac{\partial c_1}{\partial t} + U\frac{\partial c_1}{\partial x} = \frac{\partial^2 c_1}{\partial x^2} - c_1^2 - c_1 \sum_{j=1}^{\infty} a_j c_j, \quad \frac{\partial c_n}{\partial t} = a_{n-1} c_1 c_{n-1} - a_n c_1 c_n, \quad n \ge 2,$$

where $a_n = n^p$, $U = \chi f_1 / \sqrt{D\alpha C}$, and the variables are rescaled versions of the original ones.

2. CAUCHY PROBLEM

The large-time behaviour of the solution has a different form when chemotaxis is present ($U > 0$) and in the purely diffusive case ($U = 0$). In the latter case the large-time asymptotic behaviour comprises two regions. On the outer (diffusive) length scale $x = O(t^{\frac{1}{2}})$ we find a similarity solution of the form

$$(6) \qquad c_n \sim t^{-1}(\ln t)^{-n} f_n(x/t^{\frac{1}{2}}),$$

where $f_1 = \sqrt{\pi} \eta e^{-\eta^2/2} / 2a_1$ and, for $n \ge 2$,

$$(7) \qquad f_n = \frac{\pi^{n-1}}{2\eta^2 a_1^n (n-2)!} \prod_{k=1}^{n-1} a_k \int_\eta^\infty \left\{ \text{erf}\left(\frac{\hat{\eta}}{2}\right) - \text{erf}\left(\frac{\eta}{2}\right) \right\}^{n-2} \hat{\eta}^3 e^{-\frac{\hat{\eta}^2}{2}} \, d\hat{\eta}.$$

This outer solution matches with an inner solution for $x = O(1)$ of the form

$$(8) \qquad c_1 \sim \frac{C_1(x)}{t^{\frac{3}{2}} \ln t}, \qquad c_n \sim C_n(x).$$

In the case with chemotaxis ($U \neq 0$) the outer solution is of the form

$$(9) \qquad c_n \sim t^{-\frac{n+1}{2}} f_n((x - Ut)/t^{\frac{1}{2}}),$$

where $f_1(\eta)$ is the even solution of

$$(10) \qquad \frac{d^2 f_1}{d\eta^2} + \frac{\eta}{2} \frac{df_1}{d\eta} + f_1 - a_1 f_1^2 = 0,$$

with the additional condition that f_1 decays exponentially as $\eta \to \infty$. The other $f_n(\eta)$ are then given by

$$(11) \qquad f_n(\eta) = \frac{2^{n-1}}{U^{n-1}(n-2)!} \prod_{k=1}^{n-1} a_k \int_\eta^\infty \left\{ \int_\eta^{\hat{\eta}} f_1(\tilde{\eta}) \, d\tilde{\eta} \right\}^{n-2} f_1^2(\hat{\eta}) \, d\hat{\eta}.$$

For $x - Ut \gg t^{\frac{1}{2}}$, all the concentrations are exponentially small, while for $Ut - x \gg t^{\frac{1}{2}}$, c_1 is again exponentially small, but $c_n \sim C_n(x)$ for $n \geq 2$, where the $C_n(x)$ depend on the initial data. Therefore the large-time behaviour of this solution consists of an advecting peak of single cells which leaves behind itself a trail of larger clusters, with (for some constants K_n)

$$(12) \qquad C_n(x) \sim U^{\frac{n+1}{2}} K_n / x^{\frac{n+1}{2}} \qquad \text{as } x \to +\infty, \ n \geq 2.$$
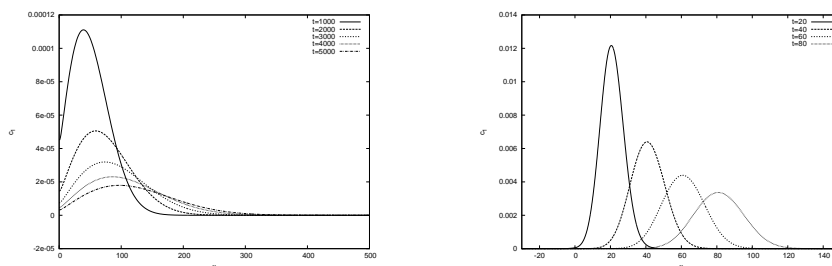
FIGURE 1. Numerical simulations for the Cauchy problem without (left) and with (right) advection.

3. CAUCHY-DIRICHLET PROBLEM

In this case we impose the Dirichlet boundary condition $c_1 = 1$ at $x = 0$. The concentrations of large clusters of cells at and near $x = 0$ increase with time, which causes the concentration of single cells to decrease rapidly away from $x = 0$. We restrict consideration to rate coefficients of the form (3), with $0 \leq p < 1$. The inner solution is the same in all cases, and is a similarity solution (in cluster-size, as well as conventional, space) of the form (defining $\xi = x t^{\frac{1}{2(1-p)}}$ and $\eta = n / t^{\frac{1}{1-p}}$)

$$(13) \qquad c_1 \sim f(\xi), \qquad c_n \sim \frac{1}{n^p} \phi(\xi, \eta),$$

and we omit further details here (the outer structure depending on the sign of U). *The authors acknowledge the support of the EPSRC for this work.*

REFERENCES

[1] D. Becker, W. Döring, Kinetische behandlung der keimbildung in übersättigten dämpfen, *Annal. Phys. (Leipzig)* **24** (1935), 719–752.
[2] E.F. Keller, L.A. Segel, Model for chemotaxis, *J. Theor. Biol.* **30** (1971), 225–234.
[3] S.L. Schor, I.R. Ellis, K. Harada, K. Motegi, A.R.A. Anderson, M.A.J. Chaplain, R.P. Keatch, A.M. Schor, A novel "sandwich" assay for quantifying chemo-regulated cell migration within 3-dimensional matrices: wound healing cytokines exhibit distinct motogenic activities compared to the transmembrane assay, *Cell Motil. Cytoskeleton* **63** (2006), 287–300.
[4] C.L. Stokes, D.A. Lauffenburger, S.K. Williams, Migration of individual microvessel endothelial cells: stochastic model and parameter measurement, *J. Cell. Sci.* **99** (1991), 419–430.

Singular limit of a reaction-diffusion system describing tissue degradation by bacteria

DANIELLE HILHORST

(joint work with John R. King, Matthias Röger)

A model for the penetration of healthy tissue by bacteria from a burn wound was proposed by John King et al. The mathematical formulation of Problem P_k is given by the parabolic equations

$$(1) \qquad \partial_t u_k \;=\; \Delta u_k - u_k + w_k - \gamma k u_k (1 - w_k) \quad \text{in} \quad Q_T$$

$$(2) \qquad \partial_t w_k \;=\; d\Delta w_k + k u_k (1 - w_k) \quad \text{in} \quad Q_T,$$

together with the boundary conditions

$$(3) \qquad \nabla u_k \cdot \vec{e}_n \;=\; 0 \quad \text{on} \quad S_T$$

$$(4) \qquad \nabla w_k \cdot \vec{e}_n \;=\; 0 \quad \text{if } d > 0 \quad \text{on} \quad S_T,$$

and the initial conditions

$$(5) \qquad u_k(0, .) \;=\; \bar{u}_0 \quad \text{in} \quad \mathbb{R}^n_+, \qquad w_k(0, .) \;=\; \bar{w}_0 \quad \text{in} \quad \mathbb{R}^n_+,$$

where

$$Q_T := (0, T) \times \mathbb{R}^n_+, \quad S_T := (0, T) \times (\mathbb{R}^{n-1} \times \{0\}),$$

with $\mathbb{R}^n_+ := \{x = (x_1, ..., x_n) \in \mathbb{R}^n : x_n > 0\}$, and $\vec{e}_n = (0, ..., 0, 1)^T$, where γ and k are positive constants and where $d \geq 0$. Here u_k corresponds to the concentration of degradative enzymes produced by the bacteria, and $1 - w_k$ corresponds to the volume fraction of healthy tissue. The key parameter $k > 0$ is typically very large and governs the degradation ratio of the tissue.

We first prove the following result

Theorem 1 *Let (u_k, w_k) be the solution of Problem (P_k) with initial data $(\bar{u}_0, \bar{w}_0)$. There exist functions $0 \le u_\infty, w_\infty \le 1$ such that*

$$u_k \to u_\infty, \quad w_k \to w_\infty \quad in \ L^1(Q_T)$$

as k tends to infinity.

In order to characterize completely the limit function pair (u_∞, w_∞), we define the functions $\varphi, h : \mathbb{R} \to \mathbb{R}$,

(6) $\qquad \varphi(r) := d(r + \gamma) + (1 - d)r_+, \qquad h(r) := \dfrac{1}{\gamma}r - (1 + \dfrac{1}{\gamma})r_+ + 1,$

where $r_+ := \max(r, 0)$ denotes the positive part of $r \in \mathbb{R}$. We set $z_0 = \bar{u}_0 - \gamma(1 - \bar{w}_0)$ and denote by z the unique weak solution of the problem P_0

(7) $\qquad\qquad \partial_t z = \Delta\varphi(z) + h(z) \qquad\qquad$ in Q_T,

(8) $\qquad\qquad \nabla\varphi(z) \cdot \vec{e}_n = 0 \qquad\qquad\qquad$ on S_T,

(9) $\qquad\qquad z(0,.) = z_0 \qquad\qquad\qquad\quad$ in $\mathbb{R}_+^n$.

Theorem 2 *The limit function pair (u_∞, w_∞) is given by $u_\infty = z_+$ and $w_\infty = 1 + (z - z_+)/\gamma$.*

Our further results deal with travelling wave solutions in the fast degradation rate limit. We consider travelling wave solutions of the one dimensional problem on the whole real line, namely solutions of the system

(10) $\qquad\qquad 0 \ = \ u'' + cu' - u + w - \gamma ku(1 - w),$

(11) $\qquad\qquad 0 \ = \ cw' + ku(1 - w).$

More precisely, we study monotone travelling waves.

Definition Let $\mathcal{K}$ be the set of functions $v \in C^\infty(\mathbb{R})$, with

(12) $\qquad\qquad\qquad 0 \ < \ v \ < \ 1, \quad v' \ < \ 0,$

(13) $\qquad\qquad\qquad v(x) \ \to \ 1, \quad$ as $x \to -\infty,$

(14) $\qquad\qquad\qquad v(x) \ \to \ 0, \quad$ as $x \to +\infty.$

We call $(c, u, w) \in \mathbb{R} \times \mathcal{K} \times \mathcal{K}$ satisfying (10), (11) a monotone (decreasing) travelling wave for (1), (2).

We prove the following results.

Theorem 3 (Existence of travelling waves) *For all γ, k there is a positive number $c_{\min} = c_{\min}(\gamma, k)$, such that there exists a monotone travelling wave of (1), (2) with speed c for all $c \geq c_{\min}$ and such there is no monotone travelling wave with speed $c < c_{\min}$.*

The value $c_{\min}$ thus gives the *minimal speed* of travelling waves for (1), (2).

Next we consider the travelling wave problem in the infinite degradation rate limit. We look for monotone travelling waves which connect one and zero, such that

$$(15) \qquad\qquad u_\infty(x), w_\infty(x) \rightarrow 1 \quad \text{as } x \rightarrow -\infty,$$

$$(16) \qquad\qquad u_\infty(x), w_\infty(x) \rightarrow 0 \quad \text{as } x \rightarrow \infty,$$

$$(17) \qquad\qquad u_\infty, w_\infty \quad \text{are decreasing.}$$

One can show that a travelling wave solution pair (u_∞, w_∞) must satisfy up to a translation constant,

$$(18) \qquad\qquad u_\infty(x) = 0 \qquad\qquad \text{for } x \geq 0,$$

$$(19) \qquad\qquad u_\infty(x) > 0, \, w_\infty(x) = 1 \qquad \text{for } x < 0,$$

together with the equations

$$(20) \qquad\qquad 0 = u_\infty'' + cu_\infty' - u_\infty + 1 \quad \text{for } x < 0,$$

$$(21) \qquad\qquad 0 = \gamma c w_\infty' + w_\infty \qquad\qquad \text{for } x > 0,$$

and the continuity and jump conditions

$$(22) \qquad\qquad u_\infty(0-) = 0,$$

$$(23) \qquad\qquad \gamma c(1 - w_\infty(0+)) = -u_\infty'(0-).$$

For all $c \geq c_\infty$, where

$$(24) \qquad\qquad c_\infty \quad := \quad \frac{1}{\sqrt{\gamma(1 + \gamma)}},$$

it turns out that there exists a unique solution (u_∞, w_∞) of (15)-(23).

Finally we prove that the travelling waves of (1), (2) are, for large values of k, close to travelling waves of the limit free boundary problem.

Theorem 4 *Let (c, u_k, w_k) be a sequence of monotone travelling waves of (1),(2) with speed $c \geq c_\infty$, such that $u_k(0) = 1/2$. As k tends to infinity, (u_k, w_k) converges to the travelling wave solution (u_∞, w_∞) of the limit free boundary problem with the same speed c.*

REFERENCES

[1] D. Hilhorst, J.R. King and M. Röger, *Mathematical Analysis of a model describing the invasion of bacteria in burn wounds*, To appear in Nonlinear Analysis TMA.

[2] D. Hilhorst, J.R. King and M. Röger, *Travelling wave analysis of a model describing the invasion of bacteria in burn wounds*, In preparation.

[3] J.R. King, A.J. Koerber, J.M. Croft, J.P. Ward, R.E. Sockett and P. Williams, *Modelling host tissue degradation by extracellular bacterial pathogens*, Mathematical Medicine and Biology **20** (2003), 227–260.

[4] J.P. Ward, J.R. King, A.J. Koerber, J.M. Croft, R.E. Sockett and P. Williams, *Cell-signalling repression in bacterial quorum sensing*, Mathematical Medicine and Biology **21** (2004), 169–204.

Remarks on three different (mathematical) aspects in chemotaxis

DIRK HORSTMANN

In 1970 E. F. Keller and L. A. Segel [7] proposed a simplified model for the aggregation process of some cellular slime models. This model was given by the following system of two strongly coupled parabolic, partial differential equations:

$$(1) \quad \left. \begin{array}{rcll} u_t & = & \nabla(k_1(u,v)\nabla u - k_2(u,v)\nabla v), & x \in \Omega, \ t > 0 \\ v_t & = & k_c\Delta v - k_3(v)v + uf(v), & x \in \Omega, \ t > 0 \\ \partial u/\partial n & = & \partial v/\partial n \ = \ 0, & x \in \partial\Omega, \ t > 0 \\ u(0,x) & = & u_0(x), \ v(0,x) \ = \ v_0(x), & x \in \Omega. \end{array} \right\}$$

Here Ω is a bounded domain $\mathbb{R}^N$ ($N \geq 1$), $u(t,x)$ denotes the myxamoebae density of the cellular slime molds and $v(t,x)$ denote a chemoattractant concentration at time t in point x.

This talk is divided in three parts, where each part gives a brief overview of one special aspect in connection with the given chemotaxis model.

PART I: BLOW-UP AND GLOBAL EXISTENCE

In their paper from 1970 E. F. Keller and L. A. Segel showed already that the uniform steady state $(\overline{u}, \overline{v})$ becomes unstable, if $\frac{k_2(\overline{u},\overline{v})\overline{v}}{k_1(\overline{u},\overline{v})\overline{u}} + \frac{\overline{u}f'(\overline{v})}{k_3(\overline{v})+\overline{v}k_3'(\overline{v})} > 1$. In the following years a discussion about the possible time asymptotic behavior of the solution started and in 1981 Childress and Percus [2] formulated for the simplified equations

$$\left. \begin{array}{rcll} u_t & = & \nabla(\nabla u - \chi u\nabla v), & x \in \Omega, \ t > 0 \\ v_t & = & k_c\Delta v - \gamma v + \alpha u, & x \in \Omega, \ t > 0 \end{array} \right\}$$

where k_c, γ, α and χ are positive constants strictly larger than zero, the following conjecture: "*In particular, for the special model we have investigated, collapse cannot occur in a one-dimensional space; may or may not in two dimensions, depending upon the cell population; and must, we surmise, in three or more dimensions under a perturbation of sufficiently high symmetry.*"

The case $N = 1$ has been analyzed and shown to be true for example in [9]. $N = 2$ has been considered in [3, 4] and finally $N \geq 3$ has been studied in [8].

However, the question arises whether this behavior is only true for the present system or whether one can show similar results for more general chemotaxis models. Therefore, Michael Winkler and myself studied in [6] chemotaxis systems where the first equation of the Keller-Segel is replaced by the more general equation $u_t = \nabla(\nabla u - f(u)\nabla v)$, where $f(u) \sim u^\beta$. We showed that:
- for $\beta < 2/N$ and $N \geq 1$ the solution exists globally in time and is uniformly bounded for all times,
- for $\beta > 2/N$ and $N \geq 1$ there exist initial data such that the solution becomes unbounded in finite or in infinite time, i. e. $\limsup_{t \to T_{max}} ||u(t, \cdot)||_{L^\infty(\Omega)} = \infty$. The borderline case $\beta = 2/N$ has only been studied for $N = 2$. Thus our results can be seen as some contribution to Childress and Percus conjecture in the case $N \geq 3$.

PART II: MULTISPECIES CHEMOTAXIS MODELS

The next question that arises is the question of multispecies chemotaxis models. In 1980 Wolfgang Alt presented in his Habilitation [1] some first models for this type of chemotaxis systems. In this talk I want to recall some results by G. Wolansky [10]. Wolansky analyzed the following generalization of the Keller-Segel model:

$$\left. \begin{array}{rcl} \nu_i u_t^i &=& \Delta u^i - \sum\limits_{j=1}^{k} \chi_{i,j} \nabla\left(u^i \nabla v^i\right), \qquad i \in \{1,...,n\} \\ \sigma_j v_t^j &=& \Delta v^j - \gamma v^j + \sum\limits_{i=1}^{n} \alpha_{i,j} u^i + f_j(x), \quad j \in \{1,...,k\} \end{array} \right\}$$

together with the boundary conditions

$$\left(\nabla u^i - \sum_{j=1}^{k} \chi_{i,j} \nabla\left(u^i \nabla v^i\right) \right) \cdot n(x) = 0 \text{ for } 1 \leq i \leq n \text{ and } v^j = 0 \text{ for } 1 \leq j \leq k.$$

Using the $n \times k$ matrices $\alpha_{i,j}$ and $\chi_{i,j}$ that describe the production and consumption rates and the mobilities of the species, he defines $\lambda_{i_1,i_2} = \sum\limits_{j=1}^{k} \chi_{i_1,j} \alpha_{i_2,j}$. The system is said to be conflict free if $\lambda_{i_1,i_2} \cdot \lambda_{i_2,i_1} > 0$ and describes chemotaxis in the presence of a conflict of interest, if $\lambda_{i_1,i_2} \cdot \lambda_{i_2,i_1} < 0$. It is shown, that there exist a Lyapunov function for conflict free systems and that there is a threshold value for the initial mass of the population densities, which decides about the time asymptotic behavior of the solution. Wolansky's results generalize the one species situation.

PART III: TRAVELING WAVES IN CHEMOTAXIS

Finally the question that arises is whether Keller-Segel type chemotaxis models can describe traveling wave like behavior of the mobile species that can be observed in several experiments. In addition to the classical results concerning that question we will present and discuss the following more general result by A. Stevens and myself [5]:

Theorem 1. *Consider for $n \geq 2$ the system*

$$(2) \quad \left.\begin{array}{rcl} u_t & = & \nabla(\nabla u - \chi \frac{u}{v} \nabla v) \\[2mm] v_t & = & k_c \Delta v + f_1 \theta \sum\limits_{j=1}^{n} a_j(jk_c - 1)u^j v^{1-j\chi} - \sum\limits_{j=1}^{n} f_1^2 a_j^2 k_c u^{2j} v^{1-2j\chi} \\[2mm] & & -2f_1^2 k_c \sum\limits_{j=3}^{2n-1} \left(\sum\limits_{\substack{k \neq l \\ k+l=j}} a_k a_l \right) u^j v^{1-j\chi}, \end{array}\right\}$$

where f_1, k_c, θ are positive and the a_j $(j \in \{1, ..., n\})$ are nonnegative constants. Then there exists a traveling wave solution for system (2), which can be explicitly calculated.

References

[1] W. Alt, *Vergleichsätze für quasilineare elliptisch-parabolische Systeme partieller Differentialgleichungen*, Habilitation, Ruprecht-Karl-Universität Heidelberg, (1980).

[2] S. Childress and J.K. Percus, *Nonlinear aspects of chemotaxis*, Math. Biosc. **56** (1981), 217–237.

[3] M.A. Herrero and J.J.L. Velázquez, *A blow-up mechanism for a chemotaxis model*, Ann. Scuola Normale Superiore **24** (1997), 633–683.

[4] D. Horstmann and G. Wang, *Blow-up in a chemotaxis model without symmetry assumptions*, Euro. J. of Applied Mathematics **12** (2001), 159–177.

[5] D. Horstmann and A. Stevens, *A constructive approach to traveling waves in chemotaxis*, J. of Nonlinear Science **14** (2004), 1–25.

[6] D. Horstmann and M. Winkler, *Boundedness vs. blow-up in a chemotaxis system*, J. Differ. Eqns **215** (2005), 52–107.

[7] E.F. Keller and L.A. Segel, *Initiation of slime mold aggregation viewed as an instability*, J. Theor. Biol. **26** (1970), 399–415.

[8] T. Nagai, *Blow-up of radially symmetric solutions to a chemotaxis system*, Adv. Math. Sci. Appl. **5** (1995), 581–601.

[9] K. Osaki and A. Yagi, *Finite dimensional attractors for one-dimensional Keller-Segel equations*, Funkcialaj Ekvacioj **44** (2001), 441–469.

[10] G. Wolansky, *Multi-components chemotactic system in absence of conflicts*, Euro. J. of Applied Mathematics **13** (2002), 641–661.

A mathematical model for stroma controlled chemotaxis of hematopoietic stem cells

Maria Neuss-Radu

(joint work with Anita Kettemann)

Hematopoietic stem cells (HSCs) are characterized by a rapid migratory activity. This property is very important for many medical applications; e.g. in the therapy of leukemia. This therapy consists in HSCs transplantation by intravenous injection of HSCs obtained from mobilized peripheral blood of the donor. After transplantation the HSCs have to find their way into their natural environment, the stem cell niche in the bone marrow consisting of so called stroma cells. This process is called homing. The aim of the physicians is to shorten the duration of the homing process as much as possible since during this time the patient is

highly endangered and the treatment is very expensive. To achieve this goal one must understand the underlying mechanism of the homing process of the HSCs and build up mathematical models able to quantify this process.

In [1] it was shown that HSCs migrate in vitro and in vivo towards a gradient of the chemotactic factor SDF-1 (stromal cell-drived factor-1) produced by the stroma cells. In a joint research project with W. Jäger (Applied Analysis) and A. Ho, R. Saffrich (Stem Cells Research) at the University of Heidelberg, we investigate the dynamics of HSCs quantitatively. In the experimental assay from [3], depicted in Fig. 1, the directed migration of HSCs toward stroma cells against a gradient of $5°$ inclination of the culture plate was observed.
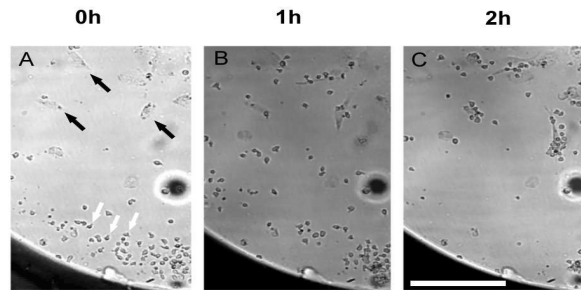
FIGURE 1. HSCs (white arrows) were initially seeded on the lower half of the Terasaki well (A). They migrated within 2 hours toward the stroma cells (black arrows) and established stable cell-cell contact with these supportive stroma cells (B,C). See [3].

Related to the experiment in [3] we came up with the following mathematical model describing the chemotactic behavior of HSCs. We consider a Lipschitz domain Ω with boundary $\partial\Omega = \Gamma_1 \cup \Gamma_2$. The boundary portion Γ_1 represents the part of the boundary where stroma cells are cultivated.

The unknowns of the model are the following,
  – $s(t,x)$ concentration of the free stem cells in the domain Ω,
  – $a(t,x)$ concentration of the chemoattractant (SDF-1),
  – $s_b(t,x)$ concentration of the stem cells bounded to the stroma cells on the boundary $\partial\Omega$.
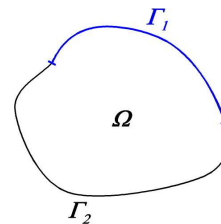
The evolution of the concentrations $s(t,x), a(t,x)$ is described by the following chemotaxis system

$$
\begin{aligned}
s_t &= \nabla \cdot (\varepsilon \nabla s - s \nabla \chi(a)), & x \in \Omega,\, t > 0 \\
a_t &= D_a \Delta a - \gamma a s, & x \in \Omega,\, t > 0.
\end{aligned}
$$

together with the boundary conditions

$$-(\varepsilon\partial_\nu s - s\chi'(a)\partial_\nu a) = \begin{cases} c_1 s - c_2 s_b & \text{on} \quad \Gamma_1, \\ 0 & \text{on} \quad \Gamma_2, \end{cases}$$

$$D_a\partial_\nu a = \begin{cases} \beta(t, s_b)c(x) & \text{on} \quad \Gamma_1, \\ 0 & \text{on} \quad \Gamma_2. \end{cases}$$

The evolution of the concentration s_b is described by the ODE

$$\partial_t s_b = c_1 s - c_2 s_b \quad \text{on} \; \Gamma_1.$$

Also we impose the initial conditions $s(0) = s_0, a(0) = a_0, s_b(0) = s_{b_0}$.

The boundary condition for the stem cells describes the absorption and desorption of the stem cells at the part of the boundary coated with stroma cells. The boundary condition for the chemoattractant models the production of the latter by the stroma cells with a rate β depending on the concentration s_b.

Remark 1. *Our choice of boundary conditions (imposed by the underlying application) makes the problem challenging from mathematical point of view. The methods used in the analysis of chemotaxis systems subjected to homogeneous Dirichlet or Neumann boundary conditions cannot be adapted to our situation.*

Theorem 1 (Existence and uniqueness of a local solution). *We assume that the data of our model satisfy the following conditions. The concentration of stroma cells c belongs to $H^{\frac{1}{2}}(\partial\Omega)$, with $0 \le c(x) \le \bar{c}$ for $x \in \Gamma_1$ and $c \equiv 0$ for $x \in \Gamma_2$. The production rate for the chemoattractant $\beta \in C^1(\mathbb{R} \times \mathbb{R}, \mathbb{R})$ satisfies*

$$0 \le \beta(t, s_b) \le M, \qquad \left|\frac{\partial\beta}{\partial s_b}(t, s_b)\right| \le M_s, \qquad \left|\frac{\partial\beta}{\partial t}(t, s_b)\right| \le M_t,$$

and the sensitivity function χ belongs to the space

$$\mathcal{S} = \left\{\chi \in C^2(\mathbb{R}) \;\middle|\; 0 \le \chi(a), \; 0 \le \chi'(a) \le C_\chi, \; |\chi''(a)| \le C'_\chi, a \in \mathbb{R}\right\}.$$

Assume also that the initial conditions are such that $s_0 \in L^\infty_+(\Omega), a_0 \in L^\infty_+(\Omega) \cap H^2(\Omega)$, and $s_{b_0} \in \{s_b \in L^\infty_+(\partial\Omega) \mid s_b(x) = 0 \text{ for } x \in \Gamma_2\} \cap H^{\frac{1}{2}}(\Gamma_1)$.

Then there exists $T > 0$ and a unique weak solution (s, a, s_b) of our system with the following properties: s, a and s_b are positive and satisfy

$$s \in L^2(0, T; H^1(\Omega)) \cap C([0, T]; L^2(\Omega)) \cap L^\infty(0, T; L^\infty(\Omega)),$$

$$s_t \in L^2(0, T; (H^1(\Omega))^*),$$

$$a \in L^2(0, T; H^2(\Omega)) \cap C([0, T]; H^1(\Omega)) \cap L^\infty(0, T; L^\infty(\Omega)),$$

$$a_t \in L^2(0, T; L^2(\Omega)),$$

$$s_b \in C([0, T]; L^2(\partial\Omega)),$$

$$(s_b)_t \in L^2(0, T; L^2(\partial\Omega)).$$

Steps of the proof: The most important steps in the proof are the following. First we cut off s in the nonlinear terms. Then we prove existence of the cut off system by Schaefer's fixed point theorem. Subsequently we show uniqueness and positivity of the solutions to the cut off system. Finally we prove boundedness for the concentration s of the cut off system in $L^\infty(0, T; L^\infty(\Omega))$ by a constant independent of the cut off constant. The details of the proof can be found in [2].

Let us now briefly describe the numerical results we obtained using the software Gascoigne, see www.gascoigne.de. We simulate our problem on a rectangle $\Omega = (0, 1.5) \times (0, 1)$ and a grid with 129×65 nodes. The time step is $\Delta t = 0.1$. We choose our data as follows. The stroma cells are concentrated on the boundary $x_1 = 1.5$ where we assume three groups of stroma cells described by $c(1.5, x_2) = 0.01(1 + 0.2\sin(5\pi x_2))$. Further we consider $\chi(a) = \chi^* a$, $D_a = 2$, $\gamma = 0.1$, $c_1 = 0.3$ and $c_2 = 0.5$. For $\beta(t, s_b)$ we choose

$$\beta(t, s_b) = V(t)\left(1 - \frac{s_b^2}{0.005 + s_b^2}\right) \text{ with } V(t) = \begin{cases} 4t^2(3 - 4t) & \text{for} \quad t \leq 0.5 \\ 1 & \text{for} \quad t > 0.5. \end{cases}$$

As initial concentrations we use $a_0(x_1, x_2) = 0$, $s_{b_0}(x_1, x_2) = 0$ and the initial function s_0 depicted in the left figure below. In the right figure below we see the distribution of the concentration s at the time step $t = 400$.
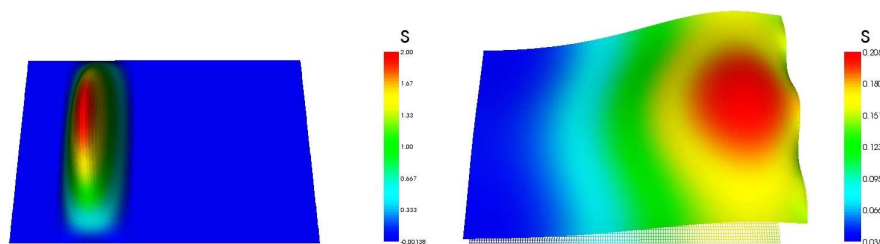
References

[1] A. Aiuti, I. J. Webb, C. Bleul, T. Springer and J. C. Gutierrez-Ramos, *The Chemokine SDF-1 Is a Chemoattractant for Human CD34$^+$ Hematopoietic Progenitor Cells and Provides a New Mechanism to Explain the Mobilization of CD34$^+$ Progenitors to Peripheral Blood*, J. Exp. Med. **185** (1997), 111–120.

[2] A. Kettemann and M. Neuss-Radu, *Analysis of a system modeling the chemotactic behavior of hematopoietic stem cells.* In preparation.

[3] W. Wagner, R. Saffrich, U. Wrikner, V. Eckstein, J. Blake, A. Ansorge, C. Schwager, F. Wein, K. Miesala, W. Ansorge and A. D. Ho, *Hematopoietic Progenitor Cells and Cellular Microenvironment: Behavioral and Molecular Changes upon Interaction*, Stem Cells **23** (2005), 1180–1191.

Travelling wave analysis for Chemotaxis with Growth

HARTMUT R. SCHWETLICK

In this article we propose a chemotaxis–growth–system for the modelling of stimulated tissue growth. Such phenomena frequently arise in wound healing and angiogenesis and used to be modeled by reaction-diffusion alone. The model focuses on the role of the epidermal growth factor in increasing mitotic activity but also serving as a chemo-attractant for the migrating cells. We show that travelling wave solutions exist, having a uniquely determined minimal wave speed depending on the diffusivity and the sensitivity of the chemotactic population. In particular, the speed is enhanced for stronger chemotactic sensitivity proposing a mechanism to increase healing rates compared to the model with purely diffusion driven migration.

In the recent modelling of wound healing or angiogenesis one describes the outer epidermal layers or highly proliferating tips of new blood vessels, see [4]. Characteristic solutions like travelling waves can provide the linkage of the microscopic but still phenomenological model to the macroscopically observables like the speed of how fast the wound closes or the blood vessel enlarges in length. Previous models use a reaction-diffusion system modelling the epidermal cell layer and the EGF growth factor concentration. However, working with parameters suggested by experiments one calculates travelling wave speeds which are to slow compared to the experiment, cf. [1].

In this work we take additionally into account that the proliferating species acts chemosensitively. Furthermore, in contrast to the chemotactic models in [2] and [3], we do distinguish between proliferating and matured cells. This is because the latter type contributes much less to the dynamic movement in the system than the first. The proposed chemotactic model provides a new alternative for the enhancement of the wave speed, thus provides a better matching with experimentally observed speeds of wound closure. We analyse the model under the assumption that diffusion of the EGF density is small compared to its degradation by the cell population, an evidence supported by the biological data, cf. the ratio $\mu = 25/13786$ given in [1, Fig. 1] for a biologically realistic parameter set.

In the following, cf. Figure 1, we denote the densities u for mobile, proliferating cells, v for the epidermal growth factor concentration, and w for adult, immobile cells.
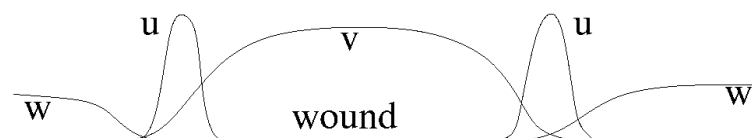
FIGURE 1. Typical shape of the profiles.

Then the chemotaxis–growth–model reads

$$(1) \quad \begin{aligned} u_t &= \nabla \cdot (d\nabla u - \chi u \nabla H(v)) + \varepsilon f(v)u, \\ v_t &= \mu \Delta v & -g(v)u, \\ w_t &= & \gamma(v,u). \end{aligned}$$

The function $f(v)$ describes the combined effect of proliferation enhanced by the presence of the growth factor v and maturation into the adult density w. We assume that if the growth is not stimulated then the rate of maturation exceeds the basic growth rate leading to the decay of the proliferating part u of the cell population. For the functional $f(v)$ this means that there exists v_0 such that f is negative for $v < v_0$ and positive for $v > v_0$. We call such a situation *monostable* since the homogeneous states ($u = 0, v = const.$) are only stable if $v < v_0$ and waves are expected to invade regions where the chemical v exceeds the threshold v_0. In contrast, the *bistable* situation describes an additional saturation effect, such that two homogeneous states ($u = 0, v_i = const.$), $i = 1, 2$ can satisfy $v_1 < v_2$ with $f(v_i) < 0$ enclosing an interval of unstable states v, i.e., $f(v) > 0$. In this case the results reveal that above unstable strip a certain range of stable states can be invaded depending on the taxis strength.

In the limit $\mu = 0$ we prove the existence of travelling waves by reducing the system with the help of a new invariant of motion along the wave coordinate. Since the reduced two-dimensional problem can be analysed exhaustively we can give a complete characterization of possible travelling waves and their speed properties.

First, let us state the result in the *monostable* case.

Theorem 2. *Let $H(v)$ be fixed. For any upstream concentration $v_+ > \gamma$ there exist planar fronts (c, u, v) for all*

$$c \geq c^* = c^*(d, \chi, \varepsilon, v_+),$$

with $u(\pm\infty) = 0$, $v(\infty) = v_+$, and $v(-\infty) = v_- = v_-(v_+)$.

Furthermore, we have bounds for the minimal speed of the waves.

Theorem 3. *There are constants $c_{0,1}(\bar{v}_+) > 0$ such that the minimal speed c^* of the front satisfies*

$$c_0 \sqrt{\varepsilon \max\{d, \chi\}} \leq c^* \leq c_1 \sqrt{\varepsilon \max\{d, \chi\}}$$

and $c^*(\cdot, \chi) \to c_0\sqrt{\gamma d}$ as $\chi \to 0$, which is the speed in the purely diffusive model.

Hence, the minimal speed gets enhanced with sufficiently strong taxis. Note, that for fixed $\chi > 0$ the wave speed stays bounded away from zero in the vanishing viscosity limit $d \to 0$. An interesting effect is that for small growth $\varepsilon \ll 1$ the model still supports waves of finite speed either if taxis χ or diffusion d is large, i.e., of order ε^{-1}.

We emphasise that the minimal speed for large taxis can not be obtained by a linear analysis of rest states but is actually a truly nonlinear phenomenon of the model. Schwetlick We shortly comment on the mechanism how waves propagate. Note that u grows ahead of the front since $v_+ > \gamma$. But the presence of u implies

annihilating v, hence, the gradient in v moves. Thus, taxis and diffusion moves the peak of u. Finally, looking downstream, we see proliferating cells mature into adult cells.

Secondly, we state the result in the *bistable* case.

Theorem 4. *Assume that f is negative for $v \notin [v_0, v_1]$. Then there exist*

(i) *monostable fronts (c, u, v) connecting $\bar{v}_+ \in (v_0, v_1]$ with $\bar{v}_- = \bar{v}_-(\bar{v}_+) < v_0$;*

(ii) *unique bistable fronts connecting any $\bar{v}_+ \in (v_1, v_\chi)$ with $\bar{v}_- = \bar{v}_-(\bar{v}_+) < v_0$, where v_χ strictly increases in χ from $v_d > v_1$ up to $v_\infty < \infty$.*

Thus, more upstream states $\bar{v}_+ > v_1$ can be invaded by travelling waves if chemotaxis is turned on and strong enough.

Remark 5. *Our analysis reveals that strong taxis χ enhances the speed for moderately diffusing cells, i.e., taxis χ takes the role of diffusivity. In the bistable model the mechanism can be used to explore the functional properties of the chemo-sensitivity model since the threshold concentration v_χ can be easily observed in experiments by analysing the macroscopic wave behaviour, i.e., checking propagation or decay.*

Now let us consider the equation for the chemical with *small* diffusion. In the monostable case we show that waves continue to exist for small positive diffusivity μ. The proof is based on geometric arguments. The abstract singular perturbation results [5] on persistence of heteroclinic orbits do not guarantee a-priorily the explicit qualitative behaviour of the travelling wave solution. We use instead a direct geometric approach to prove that orbits connect admissible equilibria while staying positive throughout. Recall that in the monostable case this condition is decisive in excluding waves having speeds lower then the minimal speed.

Theorem 6. *Assume that the growth rate f is of monostable type. Choose $\bar{v}_+ > v_0$ and $c > c^*(\bar{v}_+)$. Then there exists a small μ_0 such that for all $0 < \mu < \mu_0$ there are travelling wave solutions (u, v), u positive and v monotone, such that*

$$u(\pm\infty) = 0,$$
$$v(-\infty) = \bar{v}_-(\bar{v}_+), \quad |v(\infty) - \bar{v}_+| = O(\mu).$$

REFERENCES

[1] P.D. Dale, J.A. Sherratt and P.K. Maini, *The Speed of Corneal Epithelial Wound Healing*, Appl. Math. Lett. **7** (1994), 11–14.

[2] M. Funaki, M. Mimura and T. Tsujikawa, *Travelling front solutions arising in a chemotaxis growth model*, RIMS Kokyuroku **1135** (2002), 52–76.

[3] B.P. Marchant, J. Norbury and J.A. Sherratt, *Travelling wave solutions to a haptotaxis-dominated model of malignant invasion*, Nonlinearity **14** (2001), 1653–1671.

[4] J.A. Sherrat and J.D. Murray, *Models of epidermal wound healing*, Proc. R. Soc. Lond. B **241** (1990), 29–36.

[5] S. Wiggins, *Introduction to applied nonlinear dynamical systems and chaos*, Texts in Applied Mathematics, Springer-Verlag, New York (1990).

Dynamics of semelparous populations

Odo Diekmann

(joint work with Stephan van Gils)

A species is called "semelparous" if individuals that reproduce are bound to die (like, e.g., Pacific Salmon). If the number of years between being born and going to reproduce is fixed at, say, k years, the population decomposes into year classes according to the year of birth modulo k. The point is that such year classes are reproductively isolated, so once extinct they stay extinct. In particular, a population can consist of just a single year class, like in the case of the famous cicada's in North-America with either $k = 13$ or $k = 17$.

Year classes do, in general, interact with each other via an environmental feed-back mechanism : their survival probability and reproductive output depends on the environmental conditions (like food availability) and these, in turn, are affected by the presence or absence of other individuals.

Motivated by the single year class dynamics of cicada's, we derive and analyse replicator equations with cyclic symmetry. We then address the question : when do year classes co-exist, when does one year class outcompete all others and what other types of dynamics are possible. The main result is a classification of the repertoire of dynamical behaviour that can occur for k up to 4. Vertical bifurcations play a prominent role.

REFERENCES

[1] N.V. Davydova, O. Diekmann and S.A. van Gils, *On circulant populations I: the algebra of semelparity*, Linear Algebra and Its Applications **398** (2005), 185–243.
[2] O. Diekmann, N.V. Davydova and S.A. van Gils, *On a boom and bust year class cycle*, Journal of Difference Equations and Applications **11** (2005), 327–335.
[3] O. Diekmann and S.A. van Gils, *On the cyclic replicator equation and the dynamics of semelparous populations*, In preparation.

Stability and bifurcation analysis of models of physiologically structured populations

Mats Gyllenberg

(joint work with Odo Diekmann, Philipp Getto)

Traditionally, models of physiologically structured populations are written as hyperbolic PDEs

$$(1) \qquad \frac{\partial}{\partial t} n(t, \xi) + \nabla \cdot g(\xi, I(t)) n(t, \xi) = -\mu(\xi, I(t)), \quad \xi \in \Omega,$$

$$(2) \qquad b(t, \xi) := u \cdot g(\xi, I(t)) n(t, \xi) = \int_{\Omega} \beta(\xi, \eta, I(t)) n(t, \eta) d\eta, \quad \xi \in \partial\Omega_b.$$

Here Ω is the individual state space and $\Omega_b \subset \Omega$ is the set of all birth states. g is the individual growth rate, μ is the death rate, β the fecundity and u is the inward

normal of Ω_b. Note that the vital rates depend on the *environmental condition* (or *input*) $I(t)$, which often is of the form

$$(3) \qquad\qquad I(t) = \int_\Omega \gamma(\xi) n(t, \xi) d\xi.$$

Note that all interactions between individuals, and hence all nonlinearity is through the environment $I(t)$.

The nonlocal boundary condition (2) describes the birth rate of the population and depends on the environmental condition. As a consequence, the problem (1) – (3) is quasi-linear and hence notoriously difficult. It can be shown [3] that (1) – (3) can be written as a delay equation

$$x(t) = F(x_t), \quad t > 0 \qquad\qquad \text{(DE)}$$

for the unknown

$$(4) \qquad\qquad x(t) = \left(\begin{array}{c} b(t, \cdot) \\ I(t) \end{array} \right).$$

We shall assume that there is only a finite number of states-at-birth and that the environmental condition is finite dimensional. Then x is a function with values in $\mathbf{R}^N$. We shall also assume a maximum life span h. Then the delay equation (DE) has to be supplemented by an initial condition

$$x_0(\theta) = \varphi(\theta), \quad \theta \in [-h, 0], \qquad\qquad \text{(IC)}$$

with φ being a given function on $[-h, 0]$.

We next rewrite the system (DE) & (IC) as an abstract integral equation

$$u(t) = T_0(t)\varphi + j^{-1} \left(\int_0^t T_0^{\odot *}(t - s) G(u(s)) ds \right), \qquad\qquad \text{(AIE)}.$$

Here T_0 is the translation semigroup on $X := L^1 \left([-h, 0]; \mathbf{R}^N \right)$:

$$(5) \quad (T_0(t)\varphi)(\theta) := \begin{cases} \varphi(t + \theta) & \text{for } t + \theta \in [-h, 0], \\ 0 & \text{for } t + \theta > 0, \end{cases} \quad t \geq 0, \ \theta \in [-h, 0],$$

$T_0^{\odot *}$ is the sun-dual semigroup of T_0 acting on $X^{\odot *}$, which is represented by $\text{NBV} \left(-h, 0]; \mathbf{R}^N \right)$, j is the canonical embedding of X into $X^{\odot *}$ and G is a nonlinear mapping from X into $X^{\odot *}$ defined by

$$(6) \qquad\qquad G(\varphi) = \sum_{i=1}^N F_i(\varphi) H_i,$$

where F_i denotes the ith component of F for $i = 1, ..., N$ and H_i is defined by

$$(7) \qquad\qquad H_i(\theta) := \begin{cases} -e_i & \text{for } \theta \in (-h, 0), \\ 0 & \text{for } \theta = 0. \end{cases}$$

Here and in the sequel $\{e_1, e_2, \ldots, e_N\}$ is the standard basis of $\mathbf{R}^N$. Notice that G has finite dimensional range spanned by $\{H_1, H_2, \ldots, H_N\}$ in $X^{\odot *}$.

In [3] it was shown that the abstract integral equation (AIE) is equivalent to the problem (DE) & (IC):

Theorem 7. *Let $\varphi \in X = L^1\left([-h, 0]; \mathbf{R}^N\right)$ be given.*
(a) *Suppose that $x \in L^1_{\text{loc}}\left([-h, \infty); \mathbf{R}^N\right)$ satisfies (DE) & (IC). Then the function $u : [0, \infty) \to X$ defined by $u(t) := x_t$ is continuous and satisfies (AIE).*
(b) *Suppose that for $\varphi \in X$ there is a continuous map $u : [0, \infty) \to X$ that satisfies (AIE), then the function x defined as*

$$
(8) \qquad x(t) := \begin{cases} \varphi(t) & \text{for } t \in [-h, 0), \\ u(t)(0) & \text{for } t \geq 0 \end{cases}
$$

is an element of $L^1_{\text{loc}}\left([-h, \infty); \mathbf{R}^N\right)$ and satisfies (DE) & (IC).

The advantage of the (AIE) formulation is that there is a rich theory for such equations including the principle of linearized (in)stability; Hopf bifurcation; stable, unstable and centre manifolds. In addition, the finite dimensional range of G makes it possible to derive for each steady state of the nonlinear semigroup generated by (AIE) a characteristic equation of the form

$$
(9) \qquad \det\left(E - M(\lambda)\right) = 0,
$$

where M is an $N \times N$-matrix valued function of the complex variable λ and E is the identity matrix. The principle of linearized stability can now be formulated as follows: *If all the roots of the characteristic equation (9) lie in the left half-plane $\operatorname{Re}\lambda < 0$, then the steady state is exponentially stable, but if there is one root λ with $\operatorname{Re}\lambda > 0$, then the steady state is unstable.* It should be noted that the instability part of the principle of linearized stability has never before been proved for general physiologically structured population models.

REFERENCES

[1] Ph. Clément, O. Diekmann, M. Gyllenberg, H.J.A.M. Heijmans and H. Thieme, *Perturbation theory for dual semigroups III: Nonlinear Lipschitz continuous perturbations in the sun-reflexive case*, in: Volterra Integro-Differential Equations in Banach Spaces and Applications (G. da Prato and M. Ianelli, eds.), Pitman, Boston, (1989), 67–89.
[2] O. Diekmann, S.A. van Gils, S.M. Verduyn Lunel and H.O. Walther, "Delay Equations. Functional-, Complex-, and Nonlinear Analysis", Springer-Verlag, New York (1995).
[3] O. Diekmann, Ph. Getto and M. Gyllenberg, *Stability and bifurcation analysis of Volterra functional equations in the light of suns and stars*, submitted.

Derivation of Hyperbolic Models for Chemosensitive Movement

Francis Filbet

(joint work with Philippe Laurençot, Benoît Perthame)

A Chapman-Enskog expansion is used to derive hyperbolic models for chemosensitive movements as a hydrodynamic limit of a velocity-jump process. On the one hand, it connects parabolic and hyperbolic chemotaxis models since the former arise as diffusion limits of a similar velocity-jump process. On the other hand, this approach provides a unified framework which includes previous models obtained by *ad hoc* methods or methods of moments. Numerical simulations are also performed and are motivated by recent experiments with human endothelial cells on matrigel. Their movements lead to the formation of networks that are interpreted as the beginning of a vasculature. These structures cannot be explained by parabolic models but are recovered by numerical experiments on hyperbolic models. Our kinetic model suggests that some kind of local interactions might be enough to explain them.

In the simple situation where we only consider cells and a chemical substance (the chemo-attractant), a model for the space and time evolution of the density $n = n(t,x)$ of cells and the chemical concentration $S = S(t,x)$ at time t and position $x \in \Omega \subset \mathbb{R}^d$ has been introduced by Patlak [7] and Keller & Segel [6]. However, this approach is not always sufficiently precise to describe the evolution of bacteria movements. Indeed, experiments show that bacteria like *Escherichia Coli* move along straight lines, suddenly stop to choose a new direction and then continue moving in a new direction. This phenomenon, called run and tumble, can be modeled by a stochastic process called the velocity-jump process, and has been introduced by Alt [1] and further developed in [5, 9]. A kinetic transport model to describe this velocity jump process reads

$$(1) \qquad \frac{\partial f}{\partial t} + v \cdot \nabla_x f = \mathcal{T}(S, f),$$

where $f(t, x, v)$ denotes the density of cells, depending on time t, position x and velocity v and $\mathcal{T}$ is an operator, which models the change of direction of cells. In fact, parabolic chemotaxis equations such as the Patlak-Keller-Segel (PKS) model have been obtained as the diffusion limit of the transport equation (1). In this work, we show that hyperbolic chemotaxis models may also be derived as a fluid limit of the transport equation (1), but with a different scaling, the hydrodynamic scaling $t \to \varepsilon\, t, \quad x \to \varepsilon\, x$. The approach used relies on a Chapman-Enskog (or Hilbert) expansion and allows us to recover the previously mentioned models.

We give general assumptions on the kinetic transport model (turning operator) and use a formal Chapman-Enskog expansion to derive different hyperbolic systems which depend on the structure of the turning operator $\mathcal{T}$. We first study linear operators with respect to f and point out some of their features. We then use this approach to derive nonlinear hyperbolic models already proposed by Gamba *et al.* [8] to describe the first stages of blood vessels formation. This

approach provides a unified framework which includes previous models obtained by *ad hoc* methods or methods of moments. Finally, we perform some numerical computations of nonlinear hyperbolic models of chemotaxis, using a second order Lax-Friedrich scheme. On the one hand, we compare the transient behaviour of the parabolic model (PKS system) and hyperbolic models. Numerical simulations are also performed and are motivated by recent experiments with human endothelial cells on matrigel. Their movements lead to the formation of networks that are interpreted as the beginning of a vasculature.

In summary, chemosensitive movement models are the starting point to perform computer simulations of biological processes, which can be compared with experiments [8]. Based on these mathematical derivations at the kinetic scale and numerical simulations, this paper gives a hint that network formations for human endothelial cells on matrigel, could be also due to local interactions and not only to long range interactions. More precisely, hyperbolic models seem to represent well the phenomena and can be derived from a local interaction kernel at the kinetic level.

References

[1] W. Alt, *Biased random walk models for chemotaxis and related diffusion approximations*, J. Math. Biol. **9** (1980), 147–177.
[2] F. Filbet, Ph. Laurençot and B. Perthame, *Derivation of Hyperbolic Models for Chemosensitive Movement*, J. Math. Biol. (2005).
[3] F. Filbet and C.-W. Shu, *Approximation of Hyperbolic Models for Chemosensitive Movement*, SIAM J. Sci. Comput. (2005).
[4] A. Gamba, D. Ambrosi, A. Coniglio, A. de Candia, S. Di Talia, E. Giraudo, G. Serini, L. Preziosi and F. Bussolino, *Percolation, morphogenesis, and Burgers dynamics in blood vessels formation*, Phys. Rev. Lett. **90** (2003), 118101.
[5] T. Hillen and H.G. Othmer, *The diffusion limit of transport equations derived from velocity jump processes*, SIAM J. Appl Math. **61** (2000), 751–775.
[6] E.F. Keller and L.A. Segel, *Traveling band of chemotactic bacteria: A theoretical analysis*, J. Theor. Biol. **30** (1971), 235–248.
[7] C.S. Patlak, *Random walk with persistence and external bias*, Bull. Math. Biol. Biophys. **15** (1953), 311–338.
[8] G. Serini, D. Ambrosi, E. Giraudo, A. Gamba, L. Preziosi and F. Bussolino, *Modeling the early stages of vascular network assembly*, The EMBO Journal **22** (2003), 1771–1779.
[9] A. Stevens, *Derivation of chemotaxis-equations as limit dynamics of moderately interacting stochastic many particle systems*, SIAM J. Appl. Math. **61** (2000), 183–212.

Mathematical Modeling of Cell Movement in Fibre Networks

Thomas Hillen

In a review article on cell movement, Friedl and Bröcker [1] report that the movement of amoeboid cells on a surface differs significantly from their movement in a tissue matrix. On flat surfaces, cells appear round-shaped with broad protrusions in the direction of movement. In three dimensional tissues, however, cells

experience movement constraints given from the surrounding tissue. Some tumor cells, for example, appear elongated and spindle shaped. They send out thin pseudopods for directional guidance from the surrounding matrix. Moreover, the cells use proteases to alter the tissue and to cut through obstacles. This form of motion is termed *mesenchymal* motion [1, 2].

The main results of this work [3] are the derivation of kinetic models for mesenchymal cell movement in network tissues, their drift-diffusion scaling limits, and a discussion of the corresponding one-dimensional versions. It turns out that the macroscopic drift velocity is given by the mean tissue direction and the diffusion tensor equals the variance-covariance matrix of the directional distribution of the tissue. Both are statistically well known and experimentally measurable quantities.

The whole analysis is divided into undirected and directed tissue. In *undirected tissues* the fibres are symmetrical along their axis and both fibre directions are identical. Collagen fibres are undirected and they form the basis for many human (and animal) tissues. It is of utmost importance to understand the movement behavior of cells in tissues and to attempt to model the cell-tissue interactions.

For *directed tissues* the fibres are unsymmetrical and the two ends can be distinguished (positive/negative, forward/backward, north/south). Directed components do not play a major role for cell movement in tissues, however, directed fibres occur inside cells (such as microtubules or actin fibres) or as a combination of cells (such as the fibre tracks in the white matter of the brain). Branching collagen fibre networks can also be considered directional if the branching points are of significance for the movement of cells.

As mentioned already, the undirected case is more important for the application in mind. From the mathematical point of view, the directed case is also of interest and in this work we consider both cases. It is beneficial to have a general theory, since in the future directed fibres might be identified in the extracellular matrix (ECM) that play an important role for cell movement.

Initial numerical simulations (with K. Painter, Edinburgh and M. Preusse and C. Rohde, Bielefeld) show network forming structures for models of mesenchymal motion. Relations to vasculature formation, angiogenesis and tumour fingering are questions of ongoing research.

References

[1] P. Friedl and E.B. Bröcker, *The biology of cell locomotion within three dimensional extracellular matrix*, Cell Motility Life Sci. **57** (2000), 41–64.

[2] P. Friedl and K. Wolf, *Tumour-cell invasion and migration: diversity and escape mechanisms*, Nature Rev. **3** (2003), 362–374.

[3] T. Hillen, M^5: *Mesoscopic and Macroscopic Models for Mesenchymal Motion*, J. Math. Biol. (2006), to appear.

Cytoskeletal dynamics: (de)polymerization and crosslinking
Christian Schmeiser
(joint work with Dietmar Ölz)

The crawling movement of cells is based on the dynamics of the cell skeleton and, in particular, on the actin filament network. The observed cell morphologies and movement patterns are the result of complex interactions of the cell skeleton with a number of proteins responsible for controlling polymerization, depolymerization, cosslinking, and bundling of filaments, as well as the contact to the substrate. Another important mechanism is relative movement of filaments caused by myosin motors leading to contraction similar to muscle cells. Finally, the mechanical properties of the cell membrane and its interaction with the cytoskeleton have to be taken into account.

The present status of a modelling effort is presented, where eventually all these effects should enter into continuum models for the mechanical properties and the dynamics of the cell body derived by homogenization of descriptions on the individual filament level. At the present state, the model includes elastic properties of the filaments, a simple account of (de)polymerization, the creation and breaking of cross links, and a simple model for the mechanics of the cell membrane.

The lamellipodium is modelled as a two-dimensional structure with the actin network consisting of two families of locally parallel filaments. This assumption idealizes experimental evidence that locally two distinguished directions of filaments dominate. Each filament is modelled as a flexible, nonextensible beam. At crossings, filaments can be connected by crosslinking proteins, which provide an elastic resistance against deformation. (De-) attachment of crosslinks to the cytoskeleton network is accounted for.

Lamellipodia with the topology of a circular ring are considered, where the main part of the cell including the nucleus lies inside the inner boundary. Polymerization at the outer boundary and depolymerization at the inner boundary take place at a constant given rate at the present state of the model. The membrane is modelled as a rubber band stretched around the outer boundary.

All these ingredients are fed into an energy functional, which is time dependent by the (de)polymerization and by the (de)attachment of crosslinks. In this energy functional, a homogenization limit is carried out, where the number of filaments tends to infinity, and the spacing between locally parallel filaments tends to zero. This leads to a continuum description of the two filament families. The dynamics is assumed as quasistationary, where the energy functional is minimized at all times.

The figure shows a typical numerical solution under the assumption of rotational symmetry of the lamellipodium and with graded filament length, where all filaments are attached to the membrane and have a stochastic length distribution. By the rotational symmetry assumption, only the position of one filament (emphasized in the figure) needs to be computed. All the other positions are obtained

R$_0$=3.20, kappa^B=0.1000, kappa^S=1.0000, kappa^T=0.1000,

kappa^M=0.0001, kappa^N=1.0000, alpha=1.5708,
v$_0$=1.0000, t=5.9250, L=3.0000
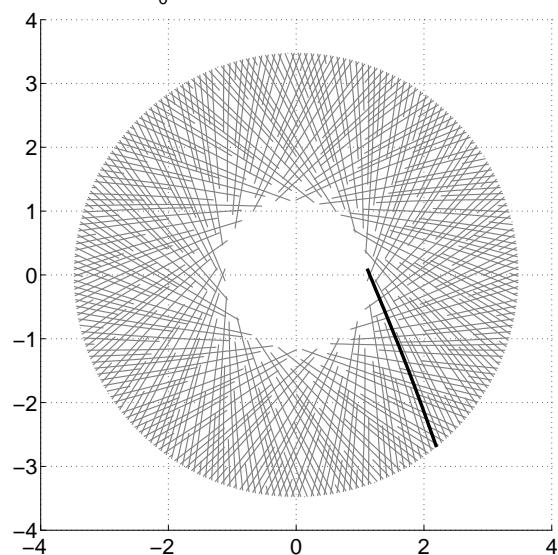
Distances from center: pointed end: 1.115, barbed end: 3.480
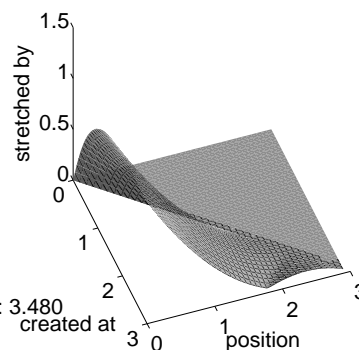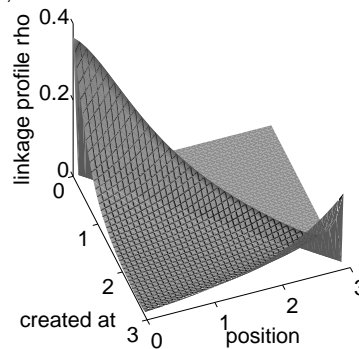
by cutting and rotating (for one family) or by flipping, cutting, and rotating (for the second family).

Reporter: Vincent Calvez

Participants

Prof. Dr. Wolfgang Alt
Institut für zelluläre & molekulare
Botanik (IZMB), Theoret. Biologie
Universität Bonn
Kirschallee 1
53115 Bonn

Prof. Dr. Alexander Anderson
Dept. of Mathematics
University of Dundee
23 Perth Road
GB-Dundee, DD1 4HN

Prof. Dr. Daniele Andreucci
Dipartimento di Metodi e Modelli
Matematici per le Scienze Applicate
Universita di Roma "La Sapienza"
Via A. Scarpa 16
I-00161 Roma

Achim Besser
Center for Modelling and Simulation
in the Biosciences (BIOMS)
Universität Heidelberg
Im Neuenheimer Feld 293
69120 Heidelberg

Dr. Vincent Calvez
Departement de Mathematiques et
Applications
Ecole Normale Superieure
45, rue d'Ulm
F-75230 Paris Cedex 05

Prof. Dr. Marie France Carlier
Laboratoire d'Enzymologie et
Biochimie Structurales
UPR 9063 Batiment 34 - CNRS
Avenue de la Terrasse
F-91198 Gif-sur-Yvette Cedex

Prof. Dr. Giovanni Caruso
Dip. di Ingegneria Civile
Universita di Roma II
Tor Vergata
I-00133 Roma

Prof. Dr. Mark Chaplain
Dept. of Mathematics
University of Dundee
23 Perth Road
GB-Dundee, DD1 4HN

Prof. Dr. Stephen H. Davis
Department of Engineering Sciences
and Applied Mathematics
Northwestern University
2145 Sheridan Road
Evanston IL 60208-3111
USA

Prof. Dr. Emmanuele DiBenedetto
Vanderbilt University
Department of Mathematics
1416 Stevenson Center
Nashville, TN 37240
USA

Prof. Dr. Richard B. Dickinson
Department of Chemical Engineering
University of Florida
P.O.Box 116005
221 Che Bldg.
Gainesville FL 32611-6005
USA

Prof. Dr. Odo Diekmann
Department of Mathematics
Utrecht University
Budapestlaan 6
NL-3584 CD Utrecht

Dr. Yasmin Dolak-Struß
Fakultät für Mathematik
Universität Wien
Nordbergstr. 15
A-1090 Wien

Elio Espejo
Max-Planck-Institut für Mathematik
in den Naturwissenschaften
Inselstr. 22 - 26
04103 Leipzig

Prof. Dr. Francis Filbet
Mathematique, Lab. MIP
Universite Paul Sabatier
118, route de Narbonne
F-31062 Toulouse Cedex

Prof. Dr. Mats Gyllenberg
Dept. of Mathematics
University of Helsinki
P.O. Box 68
FIN-00014 Helsinki

Prof. Dr. Heidi E. Hamm
Department of Cancer Biology
Vanderbilt University
Pierce Avenue 2220
Nashville, TN 37232
USA

Prof. Dr. Danielle Hilhorst
Mathematiques
Universite Paris Sud (Paris XI)
Centre d'Orsay, Batiment 425
F-91405 Orsay Cedex

Prof. Dr. Thomas Hillen
Department of Mathematical and
Statistical Sciences
University of Alberta
CAB 632
Edmonton AB T6G 2G1
Canada

Prof. Dr. I. Barry Holland
Institut de Genetique et
Microbiologie, CNRS UMR 8621
Universite Paris Sud
F-91405 Orsay Cedex

PD Dr. Dirk Horstmann
Mathematisches Institut
Universität zu Köln
50923 Köln

Prof. Dr. Hyung-Ju Hwang
Dept. of Mathematics
Trinity College
University of Dublin
Dublin 2
IRELAND

Prof. Dr. Dr. h.c. Willi Jäger
Institut für Angewandte Mathematik
Universität Heidelberg
Im Neuenheimer Feld 294
69120 Heidelberg

Prof. Dr. Anne K. Kenworthy
Vanderbilt University
School of Medicine, Department of
Molecular Physiology and Biophysics
718 Light Hall
Nashville, TN 37232
USA

Prof. Dr. David Kinderlehrer
Department of Mathematical Sciences
Carnegie Mellon University
Pittsburgh, PA 15213-3890
USA

Prof. Dr. John R. King
Dept. of Mathematics
The University of Nottingham
University Park
GB-Nottingham, NG7 2RD

Dr. Esa Kuusela
Institut für zelluläre & molekulare
Botanik (IZMB), Theoret. Biologie
Universität Bonn
Kirschallee 1
53115 Bonn

Prof. Dr. Doron Levy
Department of Mathematics
Stanford University
Stanford, CA 94305-2125
USA

Dr. Gabriela Litcanu
Institute of Applied Mathematics
and Mechanics
Warsaw University
ul. Banacha 2
02-097 Warsaw
POLAND

Dr. Thomas Lorenz
Institut für Angewandte Mathematik
Universität Heidelberg
Im Neuenheimer Feld 294
69120 Heidelberg

Dr. Anna Marciniak-Czochra
Mathematisches Institut
Universität Heidelberg
Im Neuenheimer Feld 288
69120 Heidelberg

Prof. Dr. Giovanni Naldi
Dipartimento di Matematica
Universita di Milano
Via C. Saldini, 50
I-20133 Milano

Dr. Maria Neuss-Radu
Institut für Angewandte Mathematik
Universität Heidelberg
Im Neuenheimer Feld 294
69120 Heidelberg

Prof. Dr. Hans G. Othmer
School of Mathematics
University of Minnesota
270A Vincent Hall
625-9845
Minneapolis, MN 55455
USA

Prof. Dr. Felix Otto
Institut für Angewandte Mathematik
Universität Bonn
Wegelerstr. 10
53115 Bonn

Prof. Dr. Tim J. Pedley
Department of Applied Mathematics &
Theoretical Physics (DAMTP),Centre
for Mathematical Sciences
Wilberforce Road
GB-Cambridge CB3 OWA

Prof. Dr. Benoit Perthame
Departement de Mathematiques et
Applications
Ecole Normale Superieure
45, rue d'Ulm
F-75230 Paris Cedex 05

Prof. Dr. Mathis Plapp
Laboratoire de Physique de la
Matiere Condensee
Ecole Polytechnique
F-91128 Palaiseau Cedex

Dr. Ivano Primi
Max-Planck-Institut für Mathematik
in den Naturwissenschaften
Inselstr. 22 - 26
04103 Leipzig

Prof. Dr. Vito Quaranta
Department of Cancer Biology
Vanderbilt University
Pierce Avenue 2220
Nashville, TN 37232
USA

Prof. Dr. Maria Reznikoff
Department of Mathematics
Princeton University
609 Fine Hall
Washington Road
Princeton, NJ 08544
USA

Prof. Dr. Christian Schmeiser
Fakultät für Mathematik
Universität Wien
Nordbergstr. 15
A-1090 Wien

Dr. Hartmut Schwetlick
Department of Mathematical Sciences
University of Bath
Claverton Down
GB-Bath BA2 7AY

Prof. Dr. Simone J. Seror
Institut de Genetique et
Microbiologie, CNRS UMR 8621
Universite Paris Sud
F-91405 Orsay Cedex

Prof. Dr. Angela Stevens
Max-Planck-Institut für Mathematik
in den Naturwissenschaften
Inselstr. 22 - 26
04103 Leipzig

Prof. Dr. Juan J. L. Velazquez
Matematica Aplicada
Universidad Complutense
Plaza de Ciencias 3
E-28040 Madrid

Prof. Dr. Cornelis Weijer
School of Life Sciences
University of Dundee
MSI/WTB Complex
Dow Street
GB-Dundee DD1 5EH

Prof. Dr. Hatem Zaag
Departement de Mathematiques
et Applications
Ecole Normale Superieure
45, rue d'Ulm
F-75005 Paris